An exquisite skeleton from the Middle Jurassic of Scotland illuminates an earlier origin of large pterosaurs

Natalia Jagielska[1,*], Michael O'Sullivan[2], Gregory F. Funston[1], Ian B. Butler[1], Thomas J. Challands[1], Neil D. L. Clark[3], Nicholas C. Fraser[1,4], Amelia Penny[1,5], Dugald A. Ross[6], Mark Wilkinson[1], Stephen L. Brusatte[1,4,*]

[1]School of GeoSciences, University of Edinburgh, Edinburgh, Scotland, UK

[2]Gortroe Rathkeale, Co Limerick, Ireland

[3]The Hunterian, University of Glasgow, Glasgow, Scotland, UK

[4]National Museums Scotland, Edinburgh, Scotland, UK

[5]School of Biology, University of St Andrews, Scotland, UK

[6]Staffin Museum, Staffin, Isle of Skye, Scotland, UK

[*]Correspondence

SUMMARY: Pterosaurs were the first vertebrates to evolve flight [1,2], and include the largest flying animals in Earth history[3,4]. While some of the last-surviving species were the size of aeroplanes, pterosaurs were long thought to be restricted to small body sizes (wingspans ca. <1.8-1.6 meters) from their Triassic origins through the Jurassic, before increasing in size when derived long-skulled and short-tailed pterodactyloids lived alongside a diversity of birds in the Cretaceous[5]. We report a new spectacularly preserved three-dimensional skeleton from the Middle Jurassic of Scotland, which we assign to a new genus and species *Dearc sgiathanach* gen. et sp. nov. Its wingspan is estimated at >2.5 meters, and bone histology shows it was a juvenile-subadult still actively growing when it died, making it the largest known Jurassic pterosaur represented by a well-preserved skeleton. A review of fragmentary

specimens from the Middle Jurassic of England demonstrates that a diversity of pterosaurs was capable of reaching larger sizes at this time, but have hitherto been concealed by a poor fossil record. Phylogenetic analysis places *D. sgiathanach* in a clade of basal long-tailed non-monofenestratan pterosaurs, in a subclade of larger-bodied species (Angustinaripterini) with elongate skulls convergent in some aspects with pterodactyloids[6]. Far from a static prologue to the Cretaceous, the Middle Jurassic was a key interval in pterosaur evolution, in which some non-pterodactyloids diversified and experimented with larger sizes, concurrent with or perhaps earlier than the origin of birds.

RESULTS AND DISCUSSION

Pterosauria Owen, 1842

Breviquartossa Unwin, 2003

Rhamphorhynchidae Seeley, 1870

Rhamphorhynchinae Seeley, 1870

Angustinaripterini He, 1983

Included species: *Angustinaripterus longicephalus*, *Sericipterus wucaiwanensis*, *Dearc sgiathanach* (below)

Diagnosis: group of rhamphorhynchine pterosaurs sharing a low and elongate skull (height-to-length ratio <0.2); large antorbital fenestra (20-35% skull length and >80% orbit dorsoventral height); lacrimal process of jugal nearly perpendicularly inclined (90-110^{o}) to jugal body; strongly inclined quadrate (130-140^{o} relative to maxilla long axis); cervical

vertebrae with considerable change in length-to-width ratio across the neck (1.8 to 1.2, from anterior to posterior); humeral diaphysis slender with muscle scar tubercle.

Dearc n. gen.

Type species

Dearc sgiathanach sp. nov.

Etymology

Scottish Gaelic, with the double meaning of ‘winged reptile’ and ‘reptile from Skye’, paying homage to pterosaurs (winged reptiles) and the Gaelic name for Skye (An t-Eilean Sgitheanach, the ‘winged isle’). Phonetic pronunciation: jark ski-an-ach.

Holotype

NMS (National Museums Scotland, Edinburgh) G.2021.6.1-4 (Figures 1-3), a three-dimensionally preserved articulated skeleton, lacking anterior and dorsal portions of the cranium, left manus, portions of the wings, hindlimb elements, and the distal tail. The fossil was separated into four slabs during preparation: the main slab contains the majority of bones, exposed in dorsal view (NMS G.2021.6.1), and the main counter slab contains bones exposed ventrally (NMS G.2021.6.3). An additional block contains a wing phalanx (NMS G.2021.6.4). The skull and anterior cervical vertebrae (NMS G.2021.6.2) were separated from the main slab for X-ray computed microtomography (µCT) (Figure 2).

Locality and horizon

The specimen was discovered by AP in 2017 at Rubha nam Brathairean (Brothers’ Point), Trotternish, Isle of Skye, Scotland, in the Lonfearn Member of the Lealt Shale Formation

(Bathonian, Middle Jurassic)[7,8]. The skeleton was embedded in a well-sorted lagoonal bioclastic limestone (rich in *Neomiodon*, ostracods, conchostracans), which overlies and infills dinosaur trackways impressed in subaerially exposed mudstones[9]. These units formed in a marginal marine/nearshore environment that fluctuated between submerged and exposed.

Diagnosis

Dearc sgiathanach is a rhamphorhynchine pterosaur with the following autapomorphies: tri-tubular vomers with "trident-shaped" precapillary contact; pre-choana depression on the palatal surface of the maxilla; enlarged optic lobes expanded anteroposteriorly; and fourth metatarsal more robust (diameter 2.5x) than mt1-3. For additional information, see STAR Methods.

Bone histology and maturity

Using Bennett's[10] osteologically-based ontogenetic stages for the closely related *Rhamphorhynchus*, NMS G.2021.6.1-4 has features of terminal stage adults, such as large and recurved premaxillary teeth, fused scapula-coracoid, well-developed humeral crests, smooth bone texture and fused long bone epiphyses. However, some osteological features are indicative of immaturity according to Bennett[10]: portions of the skull are unfused, such as the jugal with the pterygoid and lacrimal, and there appears to be limited fusion in the sacral vertebrae.

Immaturity is corroborated by bone histology (see STAR Methods). The cortex of a sampled wing phalanx is composed entirely of primary fibrolamellar bone[11] and preserves two prominent lines of arrested growth (LAGs), which indicate that the individual was at least two years old at death[12]. The position of the second LAG close to the external bone surface suggests that the individual died shortly after emerging from an annual growth hiatus.

The cortex is densely vascularized and has a high proportion of woven bone, indicating a rapid rate of growth throughout life[13]. The presence of vasculature extending to the external bone surface and the absence of an external fundamental system indicate that the individual was actively growing when it died. In many respects, the bone microstructure is similar to small, young individuals (< 30% adult wingspan; size class I[10]) of *Rhamphorhynchus*[14], and other actively-growing juvenile pterosaurs[15,16], indicating that it is best interpreted as a juvenile or subadult[17] that had not reached adult body size when it perished.

Wingspan and body size

Wingspan—defined as double the summed lengths of the bones of a single wing[5]—is tightly correlated to body mass and wing area in pterosaurs, and thus a robust body size proxy[18]. A complete wingspan cannot be measured directly from NMS G.2021.6.1-4 because some wing phalanges are missing. To estimate wingspan, we compiled measurements of complete wingspans of two non-monofenestratans represented by large sample sizes—*Rhamphorhynchus* and *Dorygnathus*—and regressed these against the lengths of individual bones to create predictor formulas (see STAR Methods). Using *Rhamphorhynchus* scaling, the humerus length (112 mm) and skull length (222 mm) of NMS G.2021.6.1-4 indicates wingspans of 3.8 meters and 2.2 meters, respectively. The largest known *Rhamphorhynchus* (Natural History Museum UK 37002) is considerably smaller, with a wingspan of 1.8 meters, humeral length of 79 mm, and skull length of 202 mm. Using *Dorygnathus* scaling, the humeral length of NMS G.2021.6.1-4 indicates a wingspan of 1.9 meters, approximately 10% larger than the largest *Dorygnathus* (1.69 meter wingspan, 84 mm humerus).

These results demonstrate that *Dearc* is the largest Jurassic pterosaur yet known, consistent with the fact that its humerus and skull are the longest of any Jurassic specimens. Furthermore, we interpret these results as evidence that *Dearc* likely achieved wingspans

over 2.5 meters, and perhaps larger (>3 meters). This is based on two lines of reasoning. First, we consider the *Rhamphorhynchus* equations, which give larger wingspan estimates, as the most valid predictors: *Rhamphorhynchus* is a closer relative of *Dearc* than is *Dorygnathus*; is known from a larger sample size (and thus generates a regression with tighter error bars and a higher r^2 value); and has a well-established and nearly isometric growth trajectory that makes predicting wingspan from isolated skeletal elements more justifiable[19]. Second, the holotype of *Dearc* (NMS G.2021.6.1-4) was an actively growing juvenile-subadult at death, and would have been larger as an adult (see STAR Methods).

Description

A detailed description is provided in STAR Methods, with salient features summarized here. *Dearc* generally conforms to the classic non-monofenestratan body plan, as it has an elongate mandibular symphysis (>20% mandible length), cervical ribs (visible in µCT data of anterior cervicals), a neck shorter than the combined dorsal and sacral series, a short metacarpus (<80% humerus length), and an elongate tail comprised of elongate caudal vertebrae supported by interlocking zygapophyses (Figures 1-3). It does, however, possess some features typical of pterodactyloids, and often considered part of a 'module' unique to their bauplan[6], including a skull that is longer than the combined dorsal and sacral series and a highly inclined quadrate (Figure 2). Furthermore, although the cervical vertebrae are short and squat as in non-monofenestratans, they are proportionally more elongate than most members of that grade, beginning to approach the proportions of more derived pterosaurs like *Wukongopterus lii* and *Douzhanopterus zhengi*[20,21] (see STAR Methods). There is a continuum between two distinct types of dentition: elongate fangs at the snout tip and conical pegs along much of the jaw length (Figures 2-3).

µCT data provide a stellar view of a complete, articulated palate and hyoid of a non-monofenestratan pterosaur in dorsal and ventral view (Figure 2). The heart-shaped choana is cut medially by forking vomers, comprised of three cylindrical rods that converge anteriorly in a trident-shaped contact. There is a thin extension of the ectopterygoid, which rotates around its own axis, forming an elevated ventral border of the postpalatine fenestra, joining the vomers at a perpendicular angle. This 'contorted' morphology has not been described in other pterosaurs.

µCT data also provide one of the few brain and inner ear endocasts of a basal pterosaur (Figure 2). Like *Rhamphorhynchus*[22], *Dearc* had a large cerebrum with optic lobes positioned at the same level as the forebrain and a large flocculus, around which thin and arched semicircular canals looped, that nonetheless did not project to the same lateral level as the cerebrum. In pterodactyloids, however, the brain is highly flexed so that the cerebrum is elevated relative to the optic lobes, and the flocculus is expanded beyond the cerebrum laterally[22,23,24]. In *Dearc*, the optic lobes are larger, anteroposteriorly longer, and more widely exposed dorsally than in any known basal pterosaur or pterodactyloid (*Rhamphorhynchus*[22], *Allkauren*[23], *Tapejara*[24]).

Phylogenetic analysis

Our phylogenetic analysis focuses on non-monofenestratan pterosaurs, and combines data from several independent published analyses[20,25,26,27,28,29,30,31,32,33,34,35] with new characters, while excluding taxa known only from highly immature specimens and characters that exhibit strong ontogenetic variation, resulting in a dataset of 58 taxa scored for 155 characters. *Dearc sgiathanach* is recovered within a large grade of non-monofenestratans, including subclades centred on *Rhamphorhynchus* and *Scapognathus* (Figure 4). *Dearc* is in the former subclade, where it groups with the Chinese *Angustinaripterus* and *Sericipterus*, in the clade

Angustinaripterini, diagnosed here for the first time by several features including a large antorbital fenestra, reclined quadrate, and proportionally elongate anterior cervicals (see above).

Remarks

The holotype of *Dearc sgiathanach* is a rare three-dimensionally preserved pterosaur from the Jurassic, which gives unique insight into the osteology, size, growth, and neuroanatomy of a basal non-monofenestratan. Its most remarkable attribute is its size: its wingspan was ca. 1.9–3.8 meters, roughly the size of the largest flying birds today, and it was not fully grown at death. Triassic and Jurassic pterosaurs have long been stereotyped as relatively small animals, constrained to wingspans of approximately 1.6–1.8 meters or less over the first ca. 70 million years of their evolutionary history[5], before becoming larger in the latest Jurassic or Early Cretaceous, culminating in aeroplane-sized giants like *Quetzalcoatlus* with 10-meter wingspans[5]. A few tantalizing specimens have hinted at larger Jurassic pterosaurs[36,37,38], but these are often limited to one or a few bones, which make body size estimations difficult. *Dearc* is the first Jurassic pterosaur whose wingspan can confidently be estimated at ca. 2.5 meters or greater, based on a well-preserved, articulated skeleton[5]. Its closest relatives, *Angustinaripterus* and *Sericipterus*, are also sizeable for Jurassic species, with wingspans previously estimated at 1.6[1]–1.7[38] meters extrapolated from patchy fossils. Our regression equations indicate larger wingspans for these taxa: ca. 2–3 meters, which is still approximately 10% smaller than *Dearc*. *Dearc*, therefore, anchors a clade of large, long-snouted Jurassic non-monofenestratans: Angustinaripterini[38].

The large size of *Dearc* prompted us to re-examine fragmentary specimens from the Taynton Limestone[39], an English unit that formed at the same general time as the Scottish Middle Jurassic deposits, in or along the margins of the same seaway. We identified 17

specimens—all single bones—that yield wingspan estimates of over 1.7 meters based on our predictor formulas (above), including several that may have had wingspans of over 3.0 meters. The discovery of *Dearc*, and our survey of Taynton specimens, reveals that Jurassic pterosaurs were capable of achieving considerably larger sizes than previously thought. Jurassic pterosaurs may still have been constrained in size—and certainly there is no evidence they approached the grandeur of giant Cretaceous pterodactyloids—but if so, that constraint was at a substantially greater wingspan than 1.6–1.8 meters[5].

Trends in pterosaur size evolution, particularly the shift to increasingly larger species in the Cretaceous, have been interpreted in terms of two main hypotheses, which are not mutually exclusive: 1) advances in the pterodactyloid body plan allowed them to become larger and more efficient fliers than non-pterodactyloids, and 2) the diversification of birds (Avialae)[5] may have driven latest Jurassic/Cretaceous pterosaurs into ever-larger size niches. Our identification of *Dearc* demonstrates that non-pterodactyloids were able to grow to larger sizes by the Middle Jurassic, with some evidence for large pterosaurs back to the Early Jurassic[37], tens of millions of years before birds underwent their adaptive Cretaceous radiation[40, 41]. These size increases seemingly occurred too early for avialans, which are first definitively known from the Late Jurassic, to have been a direct cause. Alternatively, if there was pressure on pterosaurs to become larger, it may have started deep in the Jurassic, and involved competition with unrecognized early avialans or other animals[40], like non-avialan feathered dinosaurs.

Not only is *Dearc* large, but it and its closest angustinaripterin relatives possess derived characters considered keystones of the pterodactyloid skull ‘module’, notably an elongate skull and inclined quadrate. Previous work has argued that the transition between non-pterodactyloids and pterodactyloids involved a nearly perfect modular shift, in which features of the skull changed together in a tightly integrated unit, followed by the body,

limbs, and tail[6]. While we do not dispute the overarching modularity of the pterosaur skeleton, *Dearc* hints that some of the trademark 'pterodactyloid' features convergently evolved in other groups[42], perhaps due to feeding ecology or other factors. Yet, the endocranial anatomy of *Dearc* is distinctly primitive, as it has the unflexed brain and smaller flocculus of basal pterosaurs[22,23] and not the transformed brain of pterodactyloids. Thus, it seems, non-pterodactyloids had a similar neuroanatomy regardless of body size.

Our recognition of large Middle Jurassic pterosaurs exposes a taphonomic bias, to add to the already notoriously problematic record of pterosaurs[43, 44]. There were fairly large pterosaurs in the Jurassic (wingspans >1.8 m), but reasonably complete adult or near-mature skeletons are mostly lacking, for reasons unclear and worthy of further study. The Middle Jurassic age of *Dearc* adds to increasing evidence that this interval—once a frustrating gap in the pterosaur record—was in fact a dynamic time of diversification, in which a variety of basal taxa and early monofenestratan lineages[6,39] coexisted and occupied a range of environments, from open marine to lagoonal, nearshore to desert, around the world. We can now add larger taxa, with derived pterodactyloid-type skull characters, to that roster. As with dinosaurs[45] and mammals[46], the Middle Jurassic was likely a vibrant time in pterosaur history, not a static and archaic prelude to a Cretaceous explosion of larger[5], more disparate[47], more efficient fliers[18]. With the dawn of the Cretaceous, however, the diverse non-monofenestratans disappeared, including larger ones with pterodactyloid convergences. This mystery remains to be solved.

ACKNOWLEDGMENTS

We thank the National Geographic Society (to PI SLB) for funding the fieldtrip on which the new pterosaur was found, a Philip Leverhulme Prize (to SLB) for funding Edinburgh's palaeontology laboratory, NERC for NJ's E4DTP studentship (NE/S007407/1), and the

Royal Society (NIF\R1\191527 to GFF) for funding the palaeohistology workspace. We thank Nigel Larkin for his expert preparation of the specimen, Stig Walsh for curation support, Elizabeth Martin-Silverstone for discussion, Scott Hartman for advice on skeletal reconstructions, and our 2017 field crew (Paige dePolo, Davide Foffa, Daniel Goldberg, Jon Hoad, Michela Johnson, Shasta Marrero, Alistair McGowan, Moji Ogunkanmi, Elsa Panciroli, Paulo Pereira, Andrew Ross, Stig Walsh, Wheelbarrow Steve). We thank Rodrigo Pêgas, David Hone, an anonymous reviewer, and editor Florian Maderspacher for their helpful comments.

AUTHOR CONTRIBUTIONS

N.J. led the study of the specimen as part of her PhD project at the University of Edinburgh and performed the descriptive and comparative analysis, assembled the character dataset and conducted the phylogenetic analysis, conducted µCT scan segmentation, drafted all figures (outlines, cladogram, reconstructions, skeleton models), and edited the text. M.O.S. provided supervision, advice on pterosaur anatomy, wingspan calculations (including the wingspan figure in Figure 4), and assistance with the phylogenetic analysis. S.L.B. supervised N.J.'s PhD project on this specimen, led the field team that collected the specimen, drafted the text of the manuscript, and performed the wingspan statistical analyses. I.B.B. µCT scanned the specimen. G.F.F. conducted the bone histology analysis and photographed the specimen. A.P. discovered the specimen. D.A.R., S.L.B., T.J.C., and A.P. collected the specimen. N.D.L.C., N.C.F., and M.W. provided co-supervision. All authors edited and approved the text.

DECLARATION OF INTERESTS

The authors declare no competing interests.

INCLUSION AND DIVERSITY

The author list of this paper includes contributors from the location where the research was conducted who participated in the data collection, design, analysis, and/or interpretation of the work.

REFERENCES

1. Wellnhofer, P. (1991). The Illustrated Encyclopedia of Pterosaurs (Salamander Books)
2. Witton M. P. (2013). Pterosaurs: Natural History, Evolution, Anatomy (Princeton University Press)
3. Lawson D. A. (1975). Pterosaur from the latest Cretaceous of West Texas: discovery of the largest flying creature. Science, 187(4180), 947-948.
4. Henderson. D. M. (2010). Pterosaur body mass estimates from three-dimensional mathematical slicing. Journal of Vertebrate Paleontology, 30(3), 768-785.
5. Benson R.B.J., Frigot R. A, Goswami A., Andres B. & Butler R. J. (2014). Competition and constraint drove Cope's rule in the evolution of giant flying reptiles. Nature communications, 5(1), 1-8.
6. Lü, J., Unwin D.M., Jin X., Liu Y., Ji Q. (2010). Evidence for modular evolution in a long-tailed pterosaur with a pterodactyloid skull. Proceedings of the Royal Society B: Biological Sciences, 277(1680), 383-389.
7. Hudson J. D. & Wakefield M. I. (2018) The Lonfearn Member, Lealt Shale Formation (Middle Jurassic) of the Inner Hebrides, Scotland. Scottish Journal of Geology, 54(2), 87-97.
8. Harris J. P. & Hudson J. D. (1980). Lithostratigraphy of the Great Estuarine Group (Middle Jurassic), Inner Hebrides. Scottish Journal of Geology, 16(2-3), 231-250.

9. dePolo P.E., Brusatte S. L., Challands T. J., Foffa D., Wilkinson M., Clark N. D. L. (2020). Novel track morphotypes from new tracksites indicate increased Middle Jurassic dinosaur diversity on the Isle of Skye, Scotland. PLoS ONE 15(3), e0229640.

10. Bennett S. C. (1995). A statistical study of *Rhamphorhynchus* from the Solnhofen Limestone of Germany: year-classes of a single large species. Journal of Paleontology, 69(3) p. 569-580.

11. Padian K., Lamm E. L. (2013). Bone histology of fossil tetrapods. (University of California Press)

12. Castanet J., Croci S., Aujard F., Perret M., Cubo J., & de Margerie E. (2004) Lines of arrested growth in bone and age estimation in a small primate: Microcebus murinus. Journal of Zoology 263, 31–39.

13. De Margerie E., Cubo J., Castanet J. (2002) Bone typology and growth rate: testing and quantifying 'Amprino's rule' in the mallard (*Anas platyrhynchos*). Comptes Rendues Biologies 325, 221–330.

14. Prondvai E., Stein K., Ősi A. & Sander M. P. (2012). Life history of *Rhamphorhynchus* inferred from bone histology and the diversity of pterosaurian growth strategies. PLoS One, 7(2), e31392.

15. Wang X., Kellner A.W., Jiang S., Cheng X., Wang Q., Ma Y., & Zhou Z. (2017). Egg accumulation with 3D embryos provides insight into the life history of a pterosaur. Science, 358(6367), 1197-1201.

16. Padian K., Horner J. R., and De Ricqlès A. (2004). "Growth in small dinosaurs and pterosaurs: the evolution of archosaurian growth strategies." Journal of Vertebrate Paleontology 24, no. 3, 555-571.

17. Woodward H.N., Freedman E. A., Farlow J.O. & Horner J.R. (2015). *Maiasaura*, a model organism for extinct vertebrate population biology: a large sample statistical assessment of growth dynamics and survivorship. Paleobiology 41(4), 503–527.

18. Venditti C., Baker J., Benton M.J., Meade A. & Humphries S. (2020). 150 million years of sustained increase in pterosaur flight efficiency. Nature, 587(7832), 83-86.

19. Hone D., Ratcliffe J. M., Riski D. K., Hermanson J. W. & Reisz R. R. (2021). Unique near isometric ontogeny in the pterosaur Rhamphorhynchus suggests hatchlings could fly. Lethaia 54, 106-112.

20. Wang X., Kellner A.W., Jiang S., Meng X, (2009). An unusual long-tailed pterosaur with elongated neck from western Liaoning of China. Anais da Academia Brasileira de Ciências, 81, 793-812.

21. Wang X., Jiang S., Zhang J., Cheng X., Yu X., Li Y., Wei G., & Wang X. (2017). New evidence from China for the nature of the pterosaur evolutionary transition. Scientific Reports 7, no. 1, 1-9.

22. Witmer L.M., Chatterjee S., Franzosa J., & Rowe T. (2003). Neuroanatomy of flying reptiles and implications for flight, posture and behaviour. Nature, 425(6961), 950-953

23. Codorniú L., Carabajal A. P., Pol D., Unwin D. & Rauhut O. W. (2016). A Jurassic pterosaur from Patagonia and the origin of the pterodactyloid neurocranium. PeerJ, 4, e2311

24. Eck K. E., Elgin R. A., Frey E. (2011). On the osteology of *Tapejara wellnhoferi* Kellner 1989 and the first occurrence of a multiple specimen assemblage from the Santana Formation, Araripe Basin, NE-Brazil. Swiss Journal of Palaeontology 130.2, 277.

25. Andres B. & Myers T. S. (2012). Lone star pterosaurs. Earth and Environmental Science Transactions of the Royal Society of Edinburgh, 103(3-4), 383-398.

26. Andres B., Clark J., & Xu X. (2014). The earliest pterodactyloid and the origin of the group. Current Biology, 24(9), 1011-1016.

27. Britt B. B., Dalla Vecchia F. M., Chure D. J., Engelmann G. F., Whiting M. F., & Scheetz E. F (2018). *Caelestiventus hanseni* gen. et sp. nov. extends the desert-dwelling pterosaur record back 65 million years. Nature ecology & evolution, 2(9), 1386-1392.

28. Dalla Vecchia F. M. (2009) Anatomy and systematics of the pterosaur *Carniadactylus* gen. n. rosenfeldi (Dalla Vecchia, 1995). Rivista Italiana di Paleontologia e stratigrafia, 115(2), 159-188.

29. Dalla Vecchia F. M. (2019). *Seazzadactylus venieri* gen. et sp. nov., a new pterosaur (Diapsida: Pterosauria) from the Upper Triassic (Norian) of northeastern Italy. PeerJ, 7, e7363.

30. Kammerer C. F., Nesbitt S. J., Flynn J.J., Ranivoharimanana L., Wyss A. R. (2020). A tiny ornithodiran archosaur from the Triassic of Madagascar and the role of miniaturization in dinosaur and pterosaur ancestry. Proceedings of the National Academy of Sciences, 117(30), 17932-17936.

31. Kellner A. W. (2003). Pterosaur phylogeny and comments on the evolutionary history of the group. Geological Society, London, Special Publications, 217(1), 105-137.

32. Lü, J., & Ji, Q (2006). Preliminary results of a phylogenetic analysis of the pterosaurs from western Liaoning and surrounding areas. Journal-paleontological society of Korea, 22(1), 239.

33. Unwin D. (2003). On the phylogeny and evolutionary history of pterosaurs. Geological Society, London, Special Publications, 217(1), 139-190.

34. Vidovic S. U. & Martill D. M (2014). *Pterodactylus scolopaciceps* Meyer, 1860 (Pterosauria, Pterodactyloidea) from the Upper Jurassic of Bavaria, Germany: the problem of cryptic pterosaur taxa in early ontogeny. PloS one 9(10), e110646.

35. Vidovic S. U. (2016). A Discourse on Pterosaur Phylogeny (Doctoral dissertation, University of Portsmouth)

36. Carpenter K., Unwin D., Cloward K., Miles C. (2003). A new scaphognathine pterosaur from the Upper Jurassic Morrison Formation of Wyoming, USA. *Geological Society, London, Special Publications*, 217(1), 45-54.

37. O'Sullivan M., Martill D. M., Groocock D. (2013). A pterosaur humerus and scapulocoracoid from the Jurassic Whitby Mudstone Formation, and the evolution of large body size in early pterosaurs. *Proceedings of the Geologists' Association*, 124(6), 973-981.

38. Andres B., Clark J. M., & Xing X. (2010). A new rhamphorhynchid pterosaur from the Upper Jurassic of Xinjiang, China, and the phylogenetic relationships of basal pterosaurs. Journal of Vertebrate Paleontology, 30(1), 163-187.

39. O'Sullivan M., Martill D. M (2018). Pterosauria of the Great Oolite Group (Bathonian, Middle Jurassic) of Oxfordshire and Gloucestershire, England. Acta Palaeontologica Polonica, 63(4).

40. Brusatte, S.L., O'Connor, J.K. and Jarvis, E.D., (2015). The origin and diversification of birds. Current Biology, 25(19), R888-R898.

41. Benson R.B. J., Choiniere J.N. (2013). Rates of dinosaur limb evolution provide evidence for exceptional radiation in Mesozoic birds. Proceedings of the Royal Society B: Biological Sciences, 280(1768)

42. Sullivan C., Yuan W., Hone D.W.E., Wang Y., Xu X., and Zhang F. (2014). The vertebrates of the Jurassic Daohugou Biota of northeastern China. *Journal of Vertebrate Paleontology* 34, no. 2, 243-280.

43. Butler R. J., Benson R. B. & Barrett P. M. (2013) Pterosaur diversity: untangling the influence of sampling biases, Lagerstätten, and genuine biodiversity signals. Palaeogeography, Palaeoclimatology, Palaeoecology, 372, 78-87.

44. Dean C.D., Mannion P. D., and Butler R.J. (2016). Preservational bias controls the fossil record of pterosaurs. Palaeontology 59, no. 2, 225-247.

45. Benson R. B. J. (2018) Dinosaur macroevolution and macroecology. Ann. Rev. Earth Plan. Sci. 49, 379-408.

46. Close R. A., Friedman M., Lloyd G. T., Benson R. B. (2015). Evidence for a mid-Jurassic adaptive radiation in mammals. Current Biology, 25(16), 2137-2142.

47. Prentice K. C., Ruta M., Benton M. J. (2011). Evolution of morphological disparity in pterosaurs. Journal of Systematic Palaeontology, 9(3), 337-353.

48. Vlassenbroeck J. (2006). Octopus 8: A High Performance Tomographic Reconstruction Package for X- ray Tube and Synchrotron micro- CT Advances in X- ray Tomography for Geomaterials, 167-173

49. Cullen T. M., Evans D.C., Ryan M. J., Currie P. J., and Kobayashi Y. (2014). Osteohistological variation in growth marks and osteocyte lacunar density in a theropod dinosaur (Coelurosauria: Ornithomimidae) BMC Evolutionary Biology 14, no. 1, 1-14.

50. Harris J. P. (1992). Mid-Jurassic lagoonal delta systems in the Hebridean basins: thickness and facies distribution patterns of potential reservoir sandbodies. Geological Society, London, Special Publications, 62(1), 111-144.

51. Morton N., Dietl G. (1989). Age of the Garantiana Clay (Middle Jurassic) in the Hebrides Basin. Scottish Journal of Geology, 25(2), 153-159.

52. Hudson J. D., Clements R. G., Riding J. B., Wakefield M. I., Walton W. (1995). Jurassic paleosalinities and brackish-water communities: a case study. Palaios, 392-407.

53. Evans S.E, Kermack K. A. (1997). Assemblages of small tetrapods from the Early Jurassic of Britain. In the shadow of the dinosaurs: early Mesozoic tetrapods. (Cambridge University Press)

54. Fraser N. C., Sues H. D. (1997). In the shadow of the dinosaurs: early Mesozoic tetrapods. (Cambridge University Press.)

55. Vincent A. J., Tyson R. V. (1999). Organic facies of the Middle Jurassic of the Inner Hebrides, Scotland. Petroleum Geoscience, 5(1), 83-92.

56. Hudson J. D., Andrews J. E. (1987). The diagenesis of the Great Estuarine Group, Middle Jurassic, Inner Hebrides, Scotland. Geological Society, London, Special Publications, 36(1), 259-276.

57. Seeley H. G. (1870). The Ornithosauria: an elementary study of the bones of pterodactyles, made from fossil remains found in the Cambridge Upper Greensand, and arranged in the Woodwardian Museum of the University of Cambridge. Deighton, Bell.

58. Plieninger, F. (1901). Beitrage zur Kenntnis der Flugsaurier. Palaeontographica 48, 65-90.

59. He X. L., Yan D., Su D. (1983). A new pterosaur from the Middle Jurassic of Dashanpu, Zigong, Sichuan. Journal of Chengdu College of Geology, 1, 27-33.

60. O'Sullivan M., Martill D.M. (2015). Evidence for the presence of *Rhamphorhynchus* (Pterosauria: Rhamphorhynchinae) in the Kimmeridge Clay of the UK. Proceedings of the Geologists' Association, 126(3), 390-401.

61. Hübner M., Gischler E., Kosma R. (2020). Rare pterosaur remains tentatively referred to *Dorygnathus banthensis* (Theodori, 1830) from the Lower Jurassic (Posidonia Shale) of Schandelah (Lower Saxony, Germany). Braunschweiger Naturkundliche Schriften, Heft 16. 2020, 2020(16), 59-82.

62. Wellnhofer P. (1975). *Die Rhamphorhynchoidea* (Pterosauria) der Oberjura-Plattenkalke Suddeutschlands. (Palaeontogr A, 148)

63. Bennett S. C. (2014). A new specimen of the pterosaur *Scaphognathus crassirostris*, with comments on constraint of cervical vertebrae number in pterosaurs. Neues Jahrbuch für Geologie und Paläontologie-Abhandlungen, 327-348.

64. Padian K. (2008). Early Jurassic pterosaur *Dorygnathus banthensis* (Theodori, 1830) and The Early Jurassic pterosaur *Campylognathoides* (Strand, 1928) Special Papers in Palaeontology (80).

65. O'Sullivan M., Martill D. M. (2013). The taxonomy and systematics of *Parapsicephalus purdoni* (Reptilia: Pterosauria) from the Lower Jurassic Whitby Mudstone Formation, Whitby, UK. Historical Biology, 29(8), 1009-1018.

66. Ősi A., Prondvai E., Frey E. B. Pohl. (2010). New interpretation of the palate of pterosaurs. The Anatomical Record: Advances in Integrative Anatomy and Evolutionary Biology, 293(2), 243-258.

67. Gasparini Z., Fernández M., Fuente M. D. L (2004). A new pterosaur from the Jurassic of Cuba. Palaeontology, 47(4), 919-927.

68. Owen R. (1859). On the vertebral characters of the order pterosauria, as exemplified in the genera *Pterodactylus* (Cuvier) and *Dimorphodon* (Owen). Philosophical Transactions of the Royal Society of London, 149, 161-169.

69. Bennett S. C. (1996). Year-classes of pterosaurs from the Solnhofen Limestone of Germany: taxonomic and systematic implications. Journal of Vertebrate Paleontology, 16(3), 432-44 4.

70. Zhou C.F. (2014). Cranial morphology of a Scaphognathus-like pterosaur, *Jianchangnathus robustus*, based on a new fossil from the Tiaojishan Formation of western Liaoning, China. Journal of Vertebrate Paleontology, 34(3), 597-605.

71. Jiang, S., Li, Z., Cheng, X. and Wang, X., (2020). The first pterosaur basihyal, shedding light on the evolution and function of pterosaur hyoid apparatuses. PeerJ, 8, p.e8292.

72. Howse S. C. B. (1986). On the cervical vertebrae of the Pterodactyloidea (Reptilia: Archosauria). Zoological Journal of the Linnean Society, 88(4), 307-328.

73. Butler R. J., Barrett P. M., Gower D. J. (2009). Postcranial skeletal pneumaticity and air-sacs in the earliest pterosaurs. Biology Letters, 5(4), 557-560.

74. Witton M. P. (2015). Were early pterosaurs inept terrestrial locomotors?. PeerJ, 3, e1018.

75. Cobb S. E & Sellers W. I. (2020). Inferring lifestyle for Aves and Theropoda: a model based on curvatures of extant avian ungual bones. Plos one, 15(2), e0211173.

76. Francillon-Vieillot H., Arntzen J. W. & Géraudie J. (1990). Age, growth and longevity of sympatric *Triturus cristatus*, *T. marmoratus* and their hybrids (Amphibia, Urodela): a skeletochronological comparison. Journal of Herpetology, 13-22.

77. Woodward H. N., Horner J. R., Farlow J. O. (2011). Osteohistological evidence for determinate growth in the American Alligator. Journal of Herpetology 45(3), 339–342.

78. Lee A. H., Werning S. (2008). Sexual maturity in growing dinosaurs does not fit reptilian growth models. Proceedings of the National Academy of Sciences (USA) 105, 582-587.

79. Calderón T., DeMiguel D., Arnold W., Stalder G., Köhler M. (2019). Calibration of life history traits with epiphyseal closure, dental eruption and bone histology in captive and wild red deer. Journal of Anatomy 235, 205–216.

77

80. Naish D., Witton M. P., Martin-Silverstone E. (2021). Powered flight in hatchling pterosaurs: evidence from wing form and bone strength. Scientific Reports, 11(1), 1-15.

81. Gross, W. (1934). Die Typen des mikroskopischen Knochenbaues bei fossilen Stegocephalen und Reptilien. Z Anat 103, 731–764.

82. Steel, L. (2008). The palaeohistology of pterosaur bone: an overview. Zitteliana, Series B, 28, 109–125.

83. Steel L. (2003). The John Quekett sections and the earliest pterosaur histological studies. Geological Society, London, Special Publications 217, no. 1, 325-334.

84. Erickson G.M, Rauhut O, Zhonghe Z., Turner A. H., Inouye B. D. (2009). Was dinosaurian physiology inherited by birds? Reconciling slow growth in Archaeopteryx. PLoS ONE 4(10), e7390.

85. Sayão J, M. (2003). Histovariability in bones of two pterodactyloid pterosaurs from the Santana Formation, Araripe Basin, Brazil: preliminary results. Geological Society of London, Special Publications 217, 335-342.

86. de Ricqlès A., Padian K., Horner J. R., Francillon-Viello, H. (2000). Paleohistology of the bones of pterosaurs (Reptilia: Archosauria): anatomy, ontogeny, and biochemical implications. Zool J Linn Soc 129, 349–385.

87. Bertozzo F., Da Silva B. C., Martill D., Marlene E. (2021). A large pterosaur femur from the Kimmeridgian, Upper Jurassic of Lusitanian Basin, Portugal. Acta Palaeontologica Polonica, *66*

FIGURE CAPTIONS

Figure 1. The new Middle Jurassic pterosaur *Dearc sgiathanach*.

Photographs of main slab (NMS G.2021.6.1-2), bones in dorsal view (A); wing phalanges 2-3 (NMS G.2021.6.3-4), in dorsal view (B); main counterslab (NMS G.2021.6.3), bones in ventral view (C). Schematic drawings (D-F) of A-C. Reconstruction of skull in dorsal (G) and ventral (I) views and skeleton in lateral view (H). Abbreviations: ar , articular region; cd, caudal vertebrae; cor, coracoid; cv, cervical vertebrae; d, digit; den, dentary; dors, dorsal vertebrae; dpc, deltopectoral crest; ep, extensor process; fm, femur; gas, gastralia; hdc, humeral distal condyle; hmt, humeral tubercle; isc, ischium; ju, jugal; max, maxilla; mc, metacarpal; mt, metatarsal; po, postorbital; r, ribs; sac, sacral plate; sca, scapula; scv, sacral (?) vertebrae; sm, sesamoid; sq, squamosal; st, sternum; symp, symphysis; uc, ulnar crest; ul, ulna; wp, wing phalanx; r/l, right/left. Blue on reconstructions are missing regions; red line on E is location of histological sectioning. Scale bars=30 mm.

Figure 2. Skull of the new Middle Jurassic pterosaur *Dearc sgiathanach*, and comparisons of pterosaur brain and ear endocasts.

Photographs (A-D), segmented µCT scan renderings (E-H), and schematic drawings (I-L) of the skull (NMS G.2021.6.2) in, from top to bottom, left lateral (reversed), dorsal, right lateral, and ventral views. Brain and inner ear endocasts (M-U) of *Rhamphorhynchus* (based on Witmer et al., 2003[22]) (M, P-Q), *Dearc* (N, R-S), and *Tapejara* (based on Eck et al., 2011[24]) (O, T-U), shown in the skull in left lateral view and isolated in left lateral and dorsal views, respectively. Abbreviations: asc, anterior semi-circular canal; bp, basisphenoid; cbl, cerebellum; cer, cerebrum; ch, choana; chl, channels; cv, third cervical; d, dentary; den, dentition; e, endocast; ec, ectopterygoid; et, edentulous anterior tip; f, frontal (?); hy, hyoid; ipv, interpterygoid vacuity; itf, inferior temporal fenestra; j, jugal; la, lacrimal; md, matrix

infilled dent; mx, maxilla; n, nasal; olf, olfactory bulb; opl, optic lobe; p, parietal; pm, premaxilla; po, postorbital; ppd, post-palatal depression; psc, posterior semi-circular canal; ptf, pneumatic foramen; q, quadrate; qj, quadrojugal; rapr, retroarticular process; rh, probable placement of rhamphotheca; sof, suborbital fenestra; sq, squamosal; sbtf, subtemporal fenestra; stf, superior temporal fenestra. In E-L, bones that cannot be distinguished in the µCT scan due to fusion or insufficient resolution are conservatively rendered together in one color. Scale bars=30 mm.

Figure 3. Postcranial skeleton and dentition of the new Middle Jurassic pterosaur *Dearc sgiathanach*.

Photographs of the right manus (A), cervical series (B), pubic region (C), right humerus (D), left humerus (E), left metacarpal-phalanx articular region (F), right maxilla (G), left pes (H) of NMS G.2021.6.1-4. Abbreviations: ac, anterior caudal vertebrae; ar, articular region; c, condyle; cdv, caudal vertebrae; cor, coracoid; cv, cervical vertebrae; d, dentary; dc, distal condyle; dpc, deltopectoral crest; dvrt, dorsal vertebrae; en, enamel; exp, extensor process; fem, femur; ft, flexor tubercle; gas, gastralia; h, humerus; ic, intercondylar groove; isc, ischium; max, maxilla; mcp, metacarpal; md, maxillary dentition; mg, medial groove; mt, metatarsal; nss, neural spine scar; pa, preacetabular process; poz, postzygapophysis ppb, prepubis; prez, prezygapophysis; rad, radius; rb, rib; sac, sacrum; sm, sesamoid; uc, ulnar crest; ul, ulna; un, ungual; vert, vertebra; wp1, wing phalanx one. Scale=10 mm per bar.

Figure 4. Phylogenetic relationships of the Middle Jurassic pterosaur *Dearc sgiathanach* and wingspan estimates for Jurassic pterosaurs.

Strict consensus of most parsimonious trees from phylogenetic analysis, with silhouettes scaled to wingspan (*Dearc*=ca. 2.0 meters) (1), and skull reconstructions of key taxa.

Wingspan plot (2), estimated wingspan range for isolated pterosaur remains from the Taynton Limestone collection. See supplementary data for complete element list. (a) NHMUK PV R 36634 (b) GSM 113726 (c)OUM J28352 (d) NHMUK PV R 38016 (e) NHMUK PV R1362 (f) LL12158 (g) NHMUK PV R 40126 (h) NMS G.2021.6.1-4 (*Dearc*) (i) OUM J23046 (k) OUM J28273 (k) NHM UK PV R 40126 B (l) OUM J28319 (m) OUM J28307 (n) OUM J28271 (o) OUM J28354 (p) LL12160 (q) OUM J23047 (r) MJM L K1995.

STAR METHODS

KEY RESOUCES TABLE

REAGENT or RESOURCE	SOURCE	IDENTIFIER
	Software and algorithms	
Avizo 9.1	Thermo Fisher Scientific	https://www.thermofisher.com/br/en/home/industrial/electron-microscopy/electron-microscopy-instruments-workflow-solutions/3d-visualization-analysis-software/avizo-materials-science.html
Mimics	Materialise	https://www.materialise.com/en/medical/mimics-innovation-suite/mimics
Trainable Weka Segmentation	ImageJ	https://imagej.net/plugins/tws/
TNT	[46]	http://www.lillo.org.ar/phylogeny/tnt/

RESOURCE AVAILABILITY

Lead contact

Further information and requests for resources should be directed to and will be fulfilled by the lead researcher Natalia Jagielska (Natalia.Jagielska@ed.ac.uk) or project supervisor Stephen L. Brusatte (Stephen.Brusatte@ed.ac.uk)

Materials availability

The holotype specimen is stored in the National Museum of Scotland (Edinburgh, Scotland, UK) under the collection number NMS G.2021.6.1-4. This is a public repository where the specimen is permanently available for research.

Data and code availability

The 3D µCT scan of the crania and cervicals can be accessed from this data repository, MorphoSource give links on publication; photogrammetric surface scan of the main slab (dorsum) is reposited in give links on publication.
The phylogenetic and wingspan analyses are included in the supplementary information and data files. The TNT matrix, measurements, segmented cranial/cervical elements are included in the Supplementary Information.

EXPERIMENTAL MODEL AND SUBJECT DETAILS

The main subject of this study, the holotype specimen NMS G.2021.6.1-4, is a well preserved, articulated, and reasonably complete skeleton preserved in a lagoonal bioclastic limestone. The exposed anterior skull of the specimen was discovered at Brothers' Point, Isle of Skye, Scotland, by AP during a National Geographic-funded fieldtrip led by SLB on May 23, 2017. The entire specimen was recovered by the team (including SLB, TJC, AP, DAR) on May 24-25, 2017. The brunt of collection work was conducted by DAR using a diamond-tipped rock saw. All fieldwork was conducted under a permit from Scottish Natural Heritage. The skeleton was found in the Upper Lonfearn Member of the Lealt Shale Formation (Great Estuarine Group), at a site that is referred to as Brothers' Point (BP) 3 in the literature[9]. BP3 is located immediately west of the mouth of Lonfearn Burn into Port Earlish (57.5863°N, 6.1494°W).

Comparative data on other specimens/taxa was retrieved from personal observations and the literature.

METHOD DETAILS

Fossil genuineness

As our team discovered the specimen in situ, we can confirm its genuineness. The specimen was mechanically prepared by Nigel Larkin, which involved gluing broken bones together and removing limestone matrix to expose the bones, but no other modifications. During collection and preparation, the fossil was separated into four slabs. The largest slab—what we refer to in the text as the 'main slab'—contains the greatest number of bones (trunk, forelimbs, sacrum and tail bones) exposed in dorsal view. The second slab—what we refer to in the text as the 'main counterslab'—includes partial trunk, tail, pelvic and hindlimb, and left forelimb elements exposed in ventral view (the underside of the slab also contains the second wing phalanx). The third slab contains the third wing phalanx with an articulation point. The fourth slab includes the skull and anterior cervical vertebrae, exposed in dorsal view. The first and second slabs were separated from each other by hammer and chisel during the removal of the skeleton from the field site. The third slab was also separated from the remainder of the skeleton during field excavation. The fourth slab was removed from the first slab by Nigel Larkin during preparation, so that it could be µCT scanned.

Fossil examination

NMS G.2021.6.1-4 was studied first-hand in the University of Edinburgh Deep Time palaeontology laboratory by many of the authors, principally NJ and SLB. The specimen was photographed by GFF and NJ using a Nikon D850 camera with Nikkor 14-24 mm and MicroNikkor 60 mm lenses. Where adjustments were made to contrast, brightness, or white balance, they were applied to the whole image. After image adjustment, the background was digitally removed. Some images were created using the automated focus-stacking mode of the Nikon D850 to create enhanced-focus images in HeliconFocus v 7.5.5.

Computed tomography scanning

The skull and associated proximal cervical vertebrae were separated from the main slab by Nigel Larkin during preparation. The skull piece was then scanned using a custom-built X-ray µCT instrument at the School of GeoSciences, University of Edinburgh. Multiple, overlapping scans of the skull were acquired at 110 keV,and 50 W target power loading with a 0.9 mm copper and 1 mm aluminium energy filter, using 2 x 2 s exposure per projection (two frames averaged) and 2000 projections per scan. The scans were reconstructed by filtered back projection using Octopus v8.9 software[48]. The geometric voxel resolution of the scans was 97µm. The overlapping scans were registered and merged into a single volume using Avizo (version 9.1) and segmented manually in Mimics (Materialize N.V. 2014). Attempts were made for machine learning segmentation using the Trainable Weka Segmentation extension on Fiji/ImageJ, but with low contrast between bone and matrix and the presence of pyrite, manual segmentation in Mimics was required. While the µCT scan offered good contrast in regions where the ratio of matrix to bone is low, contrast was reduced in the posterior part of the skull (jugal, postorbital, squamosal), and manual segmentation of this region was challenging. These segmented regions are more interpretive and low-detailed (Figure 2). Although the posterior skull has reduced contrast and resolution, the internal spaces of the brain and ear region are well defined, making it possible to produce 3D endocasts. The dorsal section of the endocast is missing due to recent beach erosion, and the terminal region anteriorly is difficult to assess as the endocast opens to the vacuity around

the orbits. The semi-circular canals can be segmented in part but are of too poor resolution to segment completely.

Bone histology

Thin sections were prepared using a modified version of the method outlined by Padian and Lamm[11]. A portion of the wing phalanx was removed at a natural break, and was embedded in Buelher Epothin II epoxy resin under a vacuum (-1 atm). The epoxy was left to cure at room temperature for 48 hours and was then cut at the target plane using a Buehler Isomet 1000 Precision Saw and a diamond-tipped wafering blade. The billet and an acrylic slide were each frosted on a glass plate using 600-grit silicon carbide abrasive slurry (Kemet International Litd.) to remove saw marks and increase surface area for adhesion. The billet was mounted to the slide using cyanoacrylate adhesive (Loctite) and was left to cure at room temperature for 3 hours. The mounted billet was resectioned to 700 µm in thickness using the Buehler Isomet 1000 Precision Saw. The section was then polished by hand on a glass plate using 600-grit silicon carbide abrasive slurry (Kemet International Litd.) until optimal contrast was achieved. The slide was finished by polishing using a 1200-grit silicon carbide abrasive slurry (Kemet International Litd.) on a glass plate, and then two 10,000-grit lapping pads (Kemet International Litd.), the second of which was impregnated with mineral oil (Johnson & Johnson) to improve optical contrast. The slide was observed and photographed using a Leica DMLP Transmitted Light Polarizing Microscope and Leica Application Suite 4. Photomontages were created using the automated 'photomerge' tool in Photoshop Creative Cloud v22.4.1. Osteocyte lacunar density was calculated using the method of Cullen et al. (2014)[49].

Wingspan estimates

In order to estimate the wingspan of NMS G.2021.6.1-4 and isolated Taynton Limestone specimens, we utilized regression equations that predict wingspan based on the dimensions of single bones. These equations were constructed using data from two genera of basal pterosaurs (non-monofenestratan species closely related to *Dearc*) known from large samples that span a range of body sizes and ontogenetic stages: *Rhamphorhynchus* and *Dorygnathus*. We compiled measurement data for specimens of these genera for which both total wingspan and the lengths of the individual bones in question can be measured. Then, for each bone, we ran a separate regression equation: one using *Rhamphorhynchus* data only, the other using *Dorygnathus* data only.

All regressions were ordinary least squares (OLS) regressions, performed in PAST, on log-transformed data. The source data for each regression, the resulting regression equations, regression plots (with 95% confidence intervals), and wingspan estimates for Dearc and isolated Taynton bones are provided in the Supplementary Excel File. Further explanation is given here:

Postcranial Bones: In order to estimate the wingspan of NMS G.2021.6.1-4 and Taynton Limestone pterosaurs, we carried out regression analyses using datasets consisting of the lengths of complete individual elements (humeri, ulnae, wing phalanges, and femora) and their corresponding complete wingspans. The humeral data were previously published in Appendix 1 of O'Sullivan et al. (2013)[37]. Each one of the Jurassic non-monofenestratan pterosaur specimens selected has at least one complete wing, which allows us to accurately measure the absolute wingspan. (Wingspan is defined as the length of one wing doubled. The body is not included as pterosaurs flew with the humerus and radius/ulna complex held in a v shape, the width of which is approximately equal to the lateral width of the body). We performed a total of 12 postcranial regressions: humerus, ulna, wing phalanx 1, wing phalanx 2, wing phalanx 4, and femur, in each case for *Rhamphorhynchus* and *Dorygnathus*

separately. In each regression, we plotted the logarithms of wingspans along the y axis against the logarithms of lengths of a complete postcranial element (e.g., humerus, wing phalanx 1, etc.) on the x axis. For each regression, we then produced a line of best fit using OLS (with 95% CIs) and measured the variance of the data using the R^2 score and the significance of the linear relationship with a permutation p value. We then took the Linear Regression Equation from our plots and used it to estimate wingspan using the formula below.

$$Wingspan = m(element\ length) + b$$

Skull: We utilized the same regression methodology to use the skull length to estimate wingspan, but using only *Rhamphorhynchus*, as too few complete skulls of *Dorygnathus* are available to conduct a robust regression analysis.

Finally, we used our postcranial and cranial regressions to estimate the wingspan of two close relatives of *Dearc*: *Sericipterus* and *Angustinaripterus*. They have been described as large Jurassic pterosaurs, but their wingspans were estimated previously at 1.6-1.7 meters based on fragmentary fossils and without explicit regression equations.

Stratigraphy, Dating, and Taphonomy

The Lealt Shale Formation is Middle Jurassic in age. It is part of a package of formations known collectively as the Great Estuarine Group, which were formed during repeated cycles of delta progradation and retrogradation into marginally marine lagoonal systems between ca. 166-170 million years ago[7]. The dating of these rocks has historically been challenging because they do not preserve ammonites—the most relevant index fossils—in abundance[7,50]. However, their stratigraphic relationships with the underlying Bajocian Garantiana Clay Member and Bearreraig Sandstone Formation and the overlying Callovian Staffin Bay Formation constrain the age range for the Great Estuarine Group—and hence the Lealt Shale—to latest Bajocian to Bathonian[50,51,52,53]. The dating of the Lealt Shale in particular has been considered Bathonian, based on correlation with neighbouring formations and the presence of ostracods in the overlying Duntulm Formation, which bear similarities to those of the *progracilis* zone[7,8]. If accurate, this would mean the Lealt Shale is coeval with the pterosaur-rich Taynton Limestone of England.

During the Bajocian-Bathonian, Britain was covered by a shallow epicontinental sea and divided into three major landmasses: London-Ardennes, Cornish-Mendip, and the northern Scottish-Pennine; the latter of which was where the Lealt Shale and other Skye deposits formed[51]. Around the end of the Bajocian, the offshore Hebridean Basin experienced sea-level rise, and became linked to neighbouring basins by flooding of low grounds, which formed shallow areas of deposition with fluctuating salinity levels[52]. These events are represented by the lagoonal/marginal marine Lealt Shale and the deltaic Valtos formations of the Great Estuarine Group, both of which are well exposed on Skye. Much of the Hebridean Basin was very shallow at this time, and submerged areas closer to shore underwent periodic drying and subaerial exposure (as evidenced by terrestrial units with dessication cracks and salt deposition)[9] . The local climate during this time was warm and humid[54].

The Lealt Shale (referred to as *Estheria* or *Mytilus* Shale in earlier literature)[8], is defined by an abrupt lithographic change from coarse-to-pebbled sandstone at the base (underlying Elgol Sandstone Formation) to bituminous, silty shale. The upper boundary is more gradational, turning from fissile muds to silts (overlying Valtos Sandstone Formation). There are notable changes in index fossils, exemplified by the disappearance of *Cyzicus* clam shrimp, and appearance of *Neomiodon* bivalve shells[51,52]. The Lealt Shale is tentatively divided into two members defined by the presence and abundance of *Mylitus* shells. The base is formed of monotypic *Praemytilus strathairdensi* shell-beds. This unit (the Kildonnan

Member) is best exposed on the Isle of Eigg, as a grey silt shale, with occasional beds of limestone, and at least two bone beds and a coarse sandstone interval. The second member—the Lonfearn—is predominately composed of shales with ostracods, gastropods and the index fossil *Cyzicus*[8] . The holotype of the new pterosaur *Dearc* comes from the Lonfearn member.

The Lonfearn member is composed of three distinctive facies[7]. The fissile mudstone facies have shell plasters, high (4.5% max.) total organic content[55] and lack bioturbation suggesting low water energy and low oxygen levels. The shell limestone facies is composed of monotaxa *Neomiodon* shell beds replaced with biosparite and displaying effects of winnowing[56], with variable levels of compaction. The new pterosaur skeleton originates from the ferruginous oolitic limestone facies, predominately composed of ooids with ferroan dolomite coating, with local muddy interbedding, pervasive fibrous calcite veins, disarticulated and winnowed bivalve shells and ostracods valves, which are found within a layer below the pterosaur specimen.

The pterosaur comes from a bed infilling sauropod trackway on a laminated micrite. It is a well-sorted, bioclastic limestone[9]. The bioclastic elements are chiefly disarticulated *Neomiodon* shells with some ostracods and conchostracans, although none have been found in the immediate vicinity of the skeleton. There are desiccation cracks present on the bed, set in some distance from the fossil, suggesting localised, periodic drying up periods in a shallow-water setting[7]. The skeleton is remarkably well preserved, with delicate and hollow bones mostly uncrushed and preserved in three dimensions, and it shows no evidence of substantial fracture, compaction, or disarticulation, suggesting it was buried in a low-energy environment, which[9] suggested as biologically active mudflats.

The rock matrix within which the pterosaur skeleton resides is rich in evenly distributed diagenetic cubic pyrite (up to 3 mm), which surrounds and in some cases (e.g., left metacarpal) extends into the fossil. The Lealt Shale Formation is intruded by numerous dolerite sills but the pterosaur skeleton has not been visibly altered by diagenesis related to magmatism and metamorphism.

Nomenclatural acts

This publication and the nomenclatural acts it contains have been registered in ZooBank under the following LSIDs: give links on publication.

Phylogenetic analysis

The phylogenetic relationships of *Dearc sgiathanach* among pterosaurs were tested using an analysis of discrete anatomical characters in a parsimony framework. The analysis includes 53 in-group terminal taxa and five outgroup taxa, scored for 155 unordered and equally weighted characters; we do not order multistate characters, to avoid any assumptions of transformation sequence. Characters include those assembled from numerous published pterosaur phylogenies and novel characters that particularly relate to features that are well preserved in *Dearc* (e.g., palatal, endocast, and ceratobranchial characters 71-79). Assembled characters originate from Andres (2012; 2014)[25,26]; Britt (2018)[27]; Dalla Vecchia (2009; 2019)[28,29]; Kammerer (2020)[30]; Kellner (2003)[31]; Lu (2006)[32]; Unwin (2003)[33]; Vidovic (2014; 2016)[34,35]; Wang (2009)[20] [details in supplementary information]. Characters exhibiting strong ontogenetic variation were excluded. Our taxon sample was constructed to focus on basal non-monofenestratan pterosaurs (the grade into which *Dearc* falls) and to mostly exclude taxa known only from immature specimens, which along with ontogenetically highly variable characters can confound phylogenetic analysis. We also excluded some taxa known only from highly incomplete or very poorly preserved specimens. We do note that we have included some taxa that are known mostly, or exclusively, from non-adult material or

have immature type specimens: most notably *Dearc* itself, but also Triassic taxa like *Eudimorphodon* and kin, and *Anurognathus*. We elected to include such taxa because of their potential phylogenetic importance (they anchor major clades or fill important gaps in the stratigraphic record) and because specimens, although immature, exhibit good preservation and completion.

Fundamentally, we acknowledge that our phylogenetic analysis relies on a series of methodological choices, and other authors may prefer alternatives. Our main goals were to focus on the relationships of non-pterodactyloids and to minimize false phylogenetic signals that could derive from immaturity and incompleteness of specimens—a long-standing problem with pterosaurs. One alternative to the latter problem is to score ontogenetic-dependent characters as missing data ('?') for species with unknown mature specimens. However, we prefer not to use this approach, because it can be challenging to recognize ontogenetic stages in pterosaurs due to the plasticity of various indicators of maturity (bone fusion and ossification, body size, histology). For instance, without our histological evidence, we would probably have considered the *Dearc* a mature (or near-mature) adult, not a still-growing juvenile or sub-adult. Given such uncertainty, we prefer the more straightforward approach of simply removing specimens/taxa known from what are clearly very immature specimens or which are highly incomplete.

We performed a maximum parsimony analysis in TNT. We began with a New Technology Search (RSS, CSS, Ratchet, Drift, Tree Fusion with default settings), in which the minimal length tree was identified 50 times. A most parsimonious tree length of 491 was found 362 times. These trees were then subjected to an additional round of TBR branch swapping, which found a total of 9000 most parsimonious trees (overflow) most parsimonious trees (consistency index=0.440, retention index=0.731). We used these trees to conduct a strict consensus in which 27 taxa were excluded a posteriori, in order to eliminate wildcard taxa and specimens with a suspected preponderance of juvenile morphological scores. Clade support was determined using Bremer and bootstrap values. The strict consensus recovered *Dearc* in a clade with *Angustinaripterus longicephalus* and *Sericipterus wucaiwanensis*; this clade is sister to *Rhamphorhynchus muenstri*.

Institutional abbreviations

BYU, Museum of Paleontology, Brigham Young University, Provo, USA; CM, Carnegie Museum of Natural History, Pittsburgh, Pennsylvania, USA; IVPP, Institute of Vertebrate Paleontology and Paleoanthropology; MCSNB, Museo Civico di Scienze Naturali di Bergamo, Bergamo (Italy); MTM, Hungarian Natural History Museum, Budapest, Hungary; NHMUK, the Natural History Museum, London, UK; NMS, National Museums Scotland, Edinburgh; OUM, Oxford University Museum of Natural History, Oxford, UK; PMOL, Paleontological Mu-seum of Liaoning, Shenyang Normal University, Shenyang, China; SMNK Staatliches Museum für Naturkunde Karlsruhe, Karlsruhe, Germany; SHN, Paleo at Sociedade de Historia Natural, Torres Vedras, Portugal; SMNS, Staatliches Museum für Naturkunde Stuttgart, Stuttgart, Germany; SNHM, State Museum of Natural History in Brunswick, Saxony, Germany; TMP, Royal Tyrrell Museum of Palaeontology, Drumheller, AB, Canada; ZDM, Zigong Dinosaur Museum.

Systematic paleontology—framework

We refer to the clade of *Dearc*, *Angustinaripterus longicephalus* and *Sericipterus wucaiwanensis* as Angustinaripterini. Due to the fast-growing pterosaur fossil record and different phylogenetic analyses and hypotheses, pterosaur clade naming conventions shift and are contested on a regular basis. *Angustinaripterus longicephalus*, known only from an elongate and sizeable crania, was placed in the undefined subfamily Angustinaripterinae by

He in the 1983 descriptive paper that established the taxon, as part of Family Rhamphorhynchidae (Seeley, 1870)[57] and Order Rhamphorhynchoidea (Plieninger, 1901)[58]. With future discoveries and revisited pterosaur phylogenies, *A. longicephalus* was found in a clade with *Harpactognathus gentryii* and *Sericipterus wucaiwanensis* in phylogenies constructed by Andres (2010)[38] and Andres et al. (2014)[26] referred to this clade with a new tribe-level name, Angustinaripterini, which they defined as 'the most inclusive clade containing *Angustinaripterus longicephalus* but not *Rhamphorhynchus muensteri*'. They did not, however, diagnose their new clade, but simply referred to it (name and definition) in a supplementary appendix. As *Dearc* possesses derived similarities with cranial elements of *A. longicephalus* and postcranial bones of *S. wucaiwanensis*, and their close relationship was corroborated by our phylogenetic analysis, we follow Andres et al. (2014)[26] in referring to this grouping as Angustinaripterini. Here, we diagnose it for the first time, ensuring its validity as a family-group taxon name under ICZN convention.

Angustinaripterini newly diagnosed clade name (tribe in Linnaean hierarchy)
Type genus
Angustinaripterus (He, 1983)[59]
Content
Angustinaripterus longicephalus, Sericipterus wucaiwanensis, Dearc sgiathanach
Stem-based definition
The most inclusive clade containing *Angustinaripterus longicephalus* but not *Rhamphorhynchus muenstri* (Andres et al., 2014)[26]
Synapomorphies
Group of rhamphorhynchine pterosaurs sharing a low and elongate skull (height to length ratio <0.2); large antorbital fenestra (20-35% skull length and >80% orbit dorsoventral height); lacrimal process of jugal nearly perpendicularly inclined (90-110^{o}) to jugal body; strongly reclined quadrate relative to other non-monofenestratans (140^{o} relative to maxilla long axis); cervical vertebrae with considerable change in length-to-width ratio across the neck (1.8 to 1.2 from anterior to posterior); humeral diaphysis slender with muscle scar tubercle medially.

***Dearc sgiathanach* gen. et sp. nov.**
Details of holotype, locality, etymology, and diagnosis in main text
Detailed diagnosis
Dearc sgiathanach is a rhamphorhynchine pterosaur with the following autapomorphies: tri-tubular vomers with "trident-shaped" precapillary contact; pre-choana depression on the palatal surface of the maxilla; enlarged optic lobes expanded anteroposteriorly; and fourth metatarsal more robust (diameter 2.5x) than mt1-3.

It furthermore possesses two characters rarely observed in other pterosaurs, which can be added to the above autapomorphies to complete a 'unique combination of characters' diagnosis: piriform inferior temporal fenestra decreasing in width dorsally; elevated ectopterygoid crossing through choana and converging on vomers at perpendicular angle.

Dearc compares to its closest relatives as detailed below. Comparisons are based on known material: *Angustinaripterus* is known from a single partial skull and dentary, *Sericipterus* from partial cranial material (rostrum and posterior dorsum) and select postcranial elements, and *Rhamphorhynchus*, *Dorygnathus* and *Scaphognathus* (including closely related *Jianchangnathus* and *Fenghuangopterus*) from a wealth of specimens of varying ontogenetic stages.

The skull of *Dearc*, despite some erosion and minor deformation, is clearly low and elongate (>0.2 length to maximum height ratio), similar to the skull of *Angustinaripterus*, but

unlike *Rhamphorhynchus*, *Scaphognathus* or *Dorygnathus*, which all have boxier, shorter crania (~0.3 length to height ratio). *Dearc* shares features of the skull openings with *Scaphognathus* and *Jianchangnathus*, namely large piriform inferior temporal fenestrae, with oblate ventral margins, and which taper dorsal. In large *Rhamphorhynchus* and *Angustinaripterus* specimens this morphology is reversed, with the tapering ventrally oriented. Also unlike large specimens of *Rhamphorhynchus*, the partially preserved ventral margin of the antorbital fenestra of *Dearc* is straight, with the underlying maxilla not fluctuating in thickness, unlike in *Rhamphorhynchus* where it is thin and increases in thickness anteriorly. The antorbital fenestra in *Angustinaripterus* makes up ~35% of total skull length, while in *Dearc* it is proportionally smaller (20%), although the anterior margin of the fenestra has been partially eroded, preventing accurate assessment. *Scaphognathus* and *Dorygnathus* have a triangulate antorbital fenestra (20% of cranial length in *Scaphognathus* and 15% in *Dorygnathus*). The lacrimal process of the jugal in both *Angustinaripterus* and *Dearc* is close to perpendicular (>110^{o}) (as measured from the long axis of jugal), and the quadrate is strongly reclined (140^{o}). In *Dorygnathus*, *Rhamphorhynchus* and *Scaphognathus*, the lacrimal process is shorter and more anteriorly leaning by <120^{o}, with less steep inclination of the quadrate (~110^{o}). The palates of *Dearc* and *Rhamphorhynchus* are highly similar, with the major dissimilarity being in the shapes of the choana and interpterygoid vacuity, as these are larger and wider in *Dearc*, which has a more defined ectopterygoid. *Rhamphorhynchus* and *Angustinaripterus* have straight mandibular rami that meet anteriorly at a robust symphysis, which makes up more than 20% of dentary length and is triangulate and sharp in ventral view; this is also the case in *Dearc*. *Scaphognathus* and *Dorygnathus* have more robust and flared symphyses. As rendered here from the CT data, the optic lobes of *Dearc* are larger and more elongate anteroposteriorly than those of *Rhamphorhynchus*, and differ from derived Cretaceous pterosaurs (like *Tapejara* SMNK PAL 1133) by having a cerebellum and flocculus positioned below the cerebrum[24]. Like *Angustinaripterus* and *Rhamphorhynchus*, the posterior (distal) maxillary teeth of *Dearc* are widely spaced, and considerably smaller compared to the more anterior (mesial) teeth, as is also visible in the rostrum of *Sericipterus* and *Rhamphorhynchus*.

As in *Sericipterus*, the cervical vertebrae of *Dearc* show a size discrepancy across the neck, with anterior cervicals being more proportionally elongate than the posterior ones. Unlike *Rhamphorhynchus*[60], the humerus of *Dearc* has a lobate deltopectoral crest that extends proximally, a sizeable ulnar crest and a slender, elongate diaphysis with a tubercle, which has been observed previously only in *Sericipterus*. Overall, the humeral morphology of *Dearc* is not dissimilar to that of *Dorygnathus*[61], albeit uniquely to *Dearc*, the deltopectoral head is taller than ulnar crest. Both *Sericipterus* and *Dearc* have a curved third wing phalanx, but in both taxa this element is strongly deformed. Unlike *Sericipterus*, *Dearc* possesses a deep medial groove on wing phalanx one, also observed in *Rhamphorhynchus*. The fourth metatarsal of *Dearc* is more than twice as thick in its diaphyseal region compared to the thinnest metatarsal. This is not the case in other pterosaurs. In *Dorygnathus* (SMNS 51827; SMNS 55886), although the distal ends of the metatarsals are flared, the diaphyseal thickness remains nearly constant. Some *Rhamphorhynchus* (NHMUK R 37002) have slender metatarsals unchanging in thickness, whereas others, like the smaller NMHUK R 2786, has a markedly thicker metatarsal I compared to II-V[62], and the same is true for *Jianchangnathus* (IVPP V16866).

Comments on systemic palaeontology

The completeness of the *Dearc* holotype allowed us to score of 111/155 characters in our phylogenetic dataset (70%). Notably, its well-preserved palate, brain and endocranial endocast and cranium provide greater morphological details than most other non-

pterodactyloid specimens. It is a non-monofenestratan pterosaur, as shown by our phylogenetic analysis. Its phylogenetic placement within derived non-pterodactyloids is supported by presence of an elongate mandibular rhamphotheca (character 26) terminating in an elongate, triangular symphysis (character 36); vertical inclination of lacrimal process of the jugal (character 49); palatal characters such as ectopterygoid perpendicular relative to medial vomers (character 73) with a narrow basipterygoid (character 74); endocasts with a cerebrum level with the flocculus (character 76); ceratobranchial length ratio to total skull length (>0.5) (character 79); shape of prepubis (character 102); numerous elongate caudal vertebrate (character 88) supported by filiform processes (character 90).

Shared characters with Angustinaripterini include: long elongate skull (character 38); variable cervical lengths (character 84); curved humeral diaphysis with dorsal muscle tubercle (character 130, 138).

Imperfect preservation obscures some traits diagnostic of non-monofenestratans. We lack the ability to measure or assess clear evidence of separation between antorbital fenestra and nares (character 60); total length of caudal vertebra (character 87); total preserved length of metacarpals and individual wing phalanges, which can be used in comparisons (Character 142 and 149); hindlimb elements, including the diagnostic digit V (character 149).

Description
(all measurements are supplied in the Excel spreadsheet in Supplementary Information)

Skull

The anterodorsal regions of the skull, particularly the snout, have been damaged by tidal erosion, and some portions are missing. An accurate complete skull length is obtainable (222 mm), and the skull is 35 mm tall at its highest undeformed point. Skull width varies from 60 mm posteriorly, 50 mm around its midpoint, and 10 mm anteriorly. The skull is triangular in dorsal view, expanding at the jugal region. Some cranial sutures are visible either externally or with µCT data, but other bones are difficult to distinguish from each other because of fusion or low µCT resolution. For example, the jugal contacts with the lacrimal and the palatal bones are clearly evident, but where the jugal meets the quadratojugal, the quadratojugal meets the quadrate, and the bones of the posterior cranium are challenging to differentiate.

The concave margins of the jugal and postorbital outline a circular orbit 38 mm in diameter, although its dorsal portion is missing due to erosion. It makes up just 20% of total skull length, located 150 mm from the anterior-most tip.

The antorbital fenestra is long (~41 mm, ~19-20% of total cranial length), has a straight ventral margin in line with the ventral margin of the orbit, and is parallel to the ventral long axis of the skull. The variable interactions between the jugal, lacrimal, maxilla and nasal results in diverse antorbital fenestra morphologies in pterosaurs, ranging from: triangulate holes smaller than the orbit in *Rhamphorhynchus*[62], *Scaphognathus*[63] and *Campylognathoides*[64], to larger and oblate openings as in *Parapsicephalus*[65] and *Dimorphodon*[68]. The sizeable, flat-ventral triangular antorbital fenestra morphology of *Dearc* is akin to that of *Scaphognathus* (in which it comprises 20% of total skull length, SMNS 59395[63]) and *Angustinaripterus* (36% of total skull length, ZDM T8001[59]). The curvature between the maxillary and lacrimal process of the jugal is more in line with *Rhamphornonychus* (CM 11431) or *Dorygnathus* (SMNS 55886) (120º). The orbit and antorbital fenestra are dorsally facing, more so than other non-pterodactyloids, although this might be due in part to the way the specimen has been eroded, and some slight compression (although, in general, the skeleton of *Dearc* is exceptionally preserved and uncrushed in three dimensions).

The maxilla is straight, with an unchanging depth of 15 mm across its a total preserved anteroposterior length of 55 mm. It bears at least 3 grooves for equally-spaced peg-like teeth (see more on the dentition below), but due to bone fusion there is no clearly visible margin between the maxilla and premaxilla or jugal. Cranial fusion displays plasticity[69], but in non-monofenestratans, this degree of fusion tends to be observed in large individuals of *Rhamphorhynchus* and *Angustinaripterus*.

The jugal is the best-preserved cranial bone. The body of the jugal beneath the orbit increases in thickness posteriorly (from 12 mm to 17 mm laterally). The lacrimal process is inclined relative to the main body of the jugal by 103º, and the postorbital process by 137º, similar to the dimensions in *Angustinaripterus*. The lacrimal process of the jugal is robust and probably reached the mid-section of the orbit. Both left and right lacrimal processes have a deep recession in the bone that does not form a fenestra, but is rather a crevice infilled with matrix; the size and shape of this crevice may be exaggerated by taphonomic alteration. The jugal extends laterally and connects to the palate with a defined, inclined margin.

Like *A. longicephalus*, *Dearc* has a strongly inclined quadrate (140º) relative to the long axis of the maxilla. The quadrate is 43 mm tall dorsoventrally and 4 mm long anteroposteriorly, and does not change considerably in thickness across its length. The quadrate is longer along its shaft than the inferior temporal fenestra it borders and ends on a globular notch overlapping with the posterior mandible. The pyriform inferior temporal fenestra (=lateral temporal fenestra) pinches out dorsally as seen in lateral view, as the ventral region is much wider anterposteriorly than the dorsal portion, and its posterior margin is flat. The inferior temporal fenestra is over 30 mm deep and 14 mm wide at its largest dimensions. The oblate tear-like shape and relative size of inferior temporal fenestra resemble that of *S. crassirostris* (SMNS 59395).

The orbit is bordered posterodorsally by the postorbital, which takes a lunate shape in dorsal view. The postorbital is 5 mm thick at its dorsal medial point. The postorbital borders the superior temporal fenestra (=supratemporal fenestra). The fenestra is 15 mm in length, is visible as a concave notch above the inferior temporal fenestra in lateral view, and is widely visible in dorsal view, where it is spherical in shape. The superior temporal fenestra is fully preserved, and makes up 9% of total skull length. The squamosal is 7 mm long in lateral view and borders the superior temporal fenestra posteriorly. The bones fold inwards to the parietal, with the symmetrical rift between the two halves at 120º. The partially preserved frontal, which is 23 mm long anteroposteriorly, is in contact with the parietal, roofing the endocranial cavity.

The skull in occipital view generally resembles *Rhamphorhynchus* (CM 11434), but due to the low resolution of the scans the bones and sutures of this complex region are difficult to unravel.

The palate of the *Dearc* holotype is exceptionally preserved in three dimensions, and has been rendered using µCT data. Previously, detailed understanding of basal pterosaur palates has been restricted to *Parapsicephalus*[65], *Dorygnathus*[64,66], *Cacibupteryx*[67] and *Rhamphorhynchus* (NHMUK R 2786[66], CM 11434[22]). The palatal region in *Dearc* is undeformed, allowing quality insight into a complete non-pterodactyloid palate, both in dorsal and ventral views. The palatal region contains a heart-shaped choana. The choana is 45 mm long and oblate, placed underneath the antorbital fenestra, and cut medially by forking vomers at 95º angle. There is a thin extension of the ectopterygoid above the postpalatine fenestra. The postpalatine fenestra measures 26-30 mm anteroposteriorly. The ectopterygoid extension is thin and slender, 27 mm long mediolaterally. The ectopterygoid rotates around its axis and cuts through the choana and marks the posterior border of the postpalatine fenestra. This trait has not been reported in other pterosaur palates, and we interpret it as autapomorphic for *Dearc*. The parasphenoid is preserved but poorly visible in the scan. The

vomer consists of three cylindrical rods, converging at an anterior point in a “trident” shaped dorsal precapillary contact. The angle between forking the vomers is 40º. There is a rectangular depression anterior to the choana. Posterior to it is a large diamond-shaped interpterygoid vacuity bordered by robust basisphenoid opening at a narrow 35º angle, the same as in *Rhamphorhynchus* (CM 11434). The surrounding pterygoid has three large, paired fenestrations, pitted with smaller fenestrations posteriorly; the three fenestrations include: a small triangular pneumatic foramen, the suborbital fenestra, and the subtemporal fenestra. The distribution and size of the fenestrae in the pterygoid is comparable to *R. muensteri* (CM 11434), in which the posterior palate is also riddled with small fenestrations. The major dissimilarity between *Dearc* and *Rhamphorhynchus* lies in the size of the choana and interpterygoid vacuity, which are larger and wider in *Dearc*. Because well preserved comparable palates are rare, and we avoid detailed comparisons with palates reconstructed from partial material (like that of *Dorygnathus*[66]), we are conservative in our assignment of autapomorphies and other diagnostic features based on the palate.

The lower jaws are preserved closed (=in occlusion with the upper skull), with the quadratojugal complex covering the jaw articulation area in lateral view. The lower jaw is a largely fused single structure, although CT data indicates that there are dorsal and ventral portions across much of the length of the element; it is currently unclear if these are due to breakage or other taphonomic forces, or represent bones of the lower jaw that have not yet fused. The jaw ramus is heavily pneumatized and the Meckelian canals terminate at the jaw mid-section. The posterior glenoid articulation forms a globular rugose surface. The jaw is straight with slight concavity (174º) along the long axis of the ramus and 185 mm in length, with an average depth of 10 mm. The left and right dentaries converge at a symphysis making up 30% of total jaw length; posteriorly they diverge from the anterior confluence point at an angle of 30º. This jaw curvature might be indicative of the specimen’s immaturity, as it has been observed in juveniles[10]. The symphysis is sharp-pointed like in *D. banthensis*[64] and *R. muensteri*[62] and not broad and flared like in *J. robustus* (PMOL-AP00028[70]) or “*Rhamphocephalus*” (GSM 113723)[39]. The symphysis terminates at an edentulous thin-walled protrusion with a pitted surface. This beak-like structure might have supported a keratinous rhamphotheca, as observed in *R. muensteri* (WDC CSG 255; MTM v 2008.33.1; and numerous others).

Two sets of ceratobranchials are preserved between the lower jaws. The ceratobranchials make up approximately 65% of the total skull length. They curve by 160º posteriorly. The brachia fold at 21º. The terminal ends are unfused to each other or other elements, and the basihyal is not preserved. The brachium is not dissimilar to that of *D. banthensis* (SMNS 50702) or *S. crassirostris* (SMNS 59395)[71], and in curvature and relative size is more similar to the latter.

Dearc displays a continuum between two distinct types of dentition: elongate fangs on the snout, and prism-shaped pegs along the side of the jaws, in the maxilla and dentary. There are no discernible changes in tooth morphology between the upper and lower jaws. The upper skull dentition extends more posteriorly than that of the lower by two pairs placed underneath the antorbital fenestra. The total number of teeth in the skull is 26. There are seven teeth in each upper jaw (the right side has a replacement tooth behind the 2nd anterior pair) and six teeth in each lower jaw. The spacing between the teeth is somewhat irregular, fluctuating between two to four alveolar spaces in the maxilla; the teeth become more packed anteriorly, with tooth roots coming to close contact in near the anterior end of the snout. The anterior teeth occlude with each other. The transverse sections of the teeth are oval in shape. The teeth are longer mesiodistally than wide labiolingually. The enamel shows evidence of taphonomic flaking; it is restricted to lower third of the tooth. The teeth have light apicobal striations, which do not affect the topography of the tooth or enamel. The teeth are vertically oriented

and the premaxillary teeth are lingually recurved, with the curvature increasing anteriorly. The dental arrangement is similar to that of adult *Rhamphorhynchus* and *Angustinaripterus*.

Axial skeleton

The *Dearc* holotype has over 25 visible individual vertebrae. The degree of completeness, articulation and deformation of each bone varies depending on the vertebral type. The neck is preserved in articulation, as is much of the tail, whereas dorsal vertebrae are less intact, and more randomly preserved, with elements scattered right and left of the trunk and pelvis of the animal, a preservation type not uncommon in other exquisitely preserved pterosaurs (like MCSNB 2888, MBR 1920.16, TMP 2008.41.001 among others).

Dearc has an almost completely preserved cervical series, starting with the fused atlas and axis with a lunate condylar articulation point in proximity to the basioccipital. The atlas-axis complex is poorly resolved in the µCT scans due to the high-density matrix, but despite this its neural canal is still visible, and the fused bones make a combined length of 31 mm. Cervicals are known for a high degree of pneumatisation, leading to frequent collapse and flattening[73], and this is true for the *Dearc* holotype. The pneumatic foramina[72,73] are generally collapsed, but often distinguishable. The positioning and shape of these features are homologous to other basal pterosaurs on record[70]. Like in *Mesadactylus* (BYU 9126), the µCT scans show a largely pneumatic cervical centrum with an oblate neural canal displaying dorsoventral flattening leading to lateral expansion. The µCT scan of the anterior cervicals uncovered pairs of cervical ribs (one to the lateral side, second to the vertebral ventral side); the ribs, as preserved, are as long as the length of the corresponding centrum. The cervical dorsal surfaces retain traces of neural spines. The anterior five cervical vertebrae, apart from the atlas-axis, are large, articulated and robust compared to the rest of the vertebral section. The anterior cervical vertebra (3, 4, 5) are elongated relative to other non-pterodactyloids (length-to-width ratio of 1.6), but the cervicals become shorter and stouter posteriorly (ratios of 1.4-1.1). Comparatively, cervicals in *Scaphognathus* (holotype and SMNS 59395) do not vary in length substantially up until a transition at cervicals 8 and 9[63], with width at 8 mm and length varying between 6.2 and 7.7 (1-1.2). In *Dorygnathus* (MBR 1920.16), cervicals three to seven are unchanging, with widths and lengths of 20 mm (ratio stays at 1), while in the basal monofenestrata *Douzhanopterus* these values vary between 2.5-3.5[21]. The prezygapophyses and postzygapophyses are generally preserved, and articulation areas associated with the condyles and cotyles retain a rugose texture. There is a short (3 mm) bi-condylar protrusion below the centrum of vertebra 3, which can be considered as a postexapophysis. This feature is not frequently found in non-pterodactyloids, save from IVPP V14725 (*S. wucaiwanensis*) and NHMUK PV R 40126a (assigned as belonging to a basal monofenestratan). Andres[38] suggested the presence of postexapophyses correlated with an increase of cervical size, while O'Sullivan[39] suggested the feature might be associated with pterodactyloid modular development. *S. wucaiwanensis* similarly displays a strong discrepancy in cervical vertebral dimensions, with cervical vertebra 3 bearing dimensions of 22.3 by 15.1 (mm), while vertebra 8 is 22.5 by 25.2 (mm)[38].

The dorsal vertebrae are preserved on the main counterslab. The dorsal vertebrae show less morphological variation and experience less flattening than the cervical vertebrae. The dorsal vertebrae are hour-glass shaped, composed of a slender vertebral body with wider terminal ends which appear to be symmetrical at the medial section. The dorsal vertebrae are associated with a scattering of disarticulated dorsal ribs (see below).

Dearc has a poorly preserved sacrum. The pelvis is deformed and exposed in relatively uninformative ventral view, preventing sound assessment of the transition between the dorsal and unfused sacral vertebra, and thus a reliable sacral count. There are 13 observable dorsal and sacral vertebrae, in total. The combined dorsal-sacral region measures

~195mm, which is longer than the total of cervical series and nearly equal in length to the skull.

Dearc has over ten caudal vertebrae. The first three preserved vertebrae are squat and square, transitioning into more elongate vertebrae, stiffened by numerous interlocking zygapophyses and filiform processes, preserved as stacks of long, thin in impressions flanking the vertebral centra. The bones become obscured by transverse processes distally, making it hard to distinguish individual vertebrae. Clearly the total length of the tail is at least 190 mm, but because distal parts of the tail are obscured by limestone and a calcite vein, the entire tail is likely longer.

The best-preserved and most robust dorsal ribs are the anterior pair, which lie near the shoulder blades. The ribs retain a boot-shaped, concave articular facet close to the rib head, with a medial coastal groove (visible on 2nd left and 3rd right ribs). An anterior rib is 10 mm wide at its head, 4 mm proximally, reducing to less than 2 mm distally; no rib is preserved in full. The rib is concave (160^{o}). There are around 20 featureless long bones spread across the slab, and these bony elements have widths varying from 2 to 1 mm and are slightly concave. Many cluster anterior to the pre-pubis, and are possibly remnants of the gastral basket. The sternal ribs with characteristic monocondylar sternocostal joints (as observed in *Rhamphorhynchus*) are not visible.

The axial skeleton in *Dearc* is strongly indicative of its non-pterodactyloid identification. These features include: cervical ribs, short cervical vertebrae with the total cervical series shorter than the dorsals and sacrals combined, and an elongate tail supported by interlocking processes. There are interesting points of deviation from the classic non-pterodactyloid body plan, however, in the relatively long skull relative to the dorsal-sacral series, anterior cervical elongation and the presence of postexapophyses. These are features more traditionally seen in the pterodactyloid body plan[6].

Appendicular skeleton: pectoral girdle and forelimbs

The wings are well preserved, but no single wing is complete. In total, the specimen bears two intact humeri, a partial albeit measurable ulna and radius and metacarpals on the right side, partial antebrachium elements on the left side, and many wing (4th digit) phalanges. No wing phalanx is complete. The humerus is 112 mm long; the metacarpus and radius/ulna combined are ca. 200 mm long (with metacarpus and syncarpals making approximately 40-75 mm of that value). Wing phalanx one is preserved on both right and left sides, the left being better preserved, with a total (preserved) length of 110 mm; phalanx two (right) is greater than 135 mm long; the third is greater than 129 mm long, and the terminal phalanx is missing. The humerus (and skull length) allow reasonable wingspan estimates, and the sheer size of the partially preserved wing bones—and the entire skeleton itself—immediately corroborate the fact that this is a large specimen for a Jurassic-aged pterosaur.

The scapulocoracoids are preserved at an inaccessible angle with only proximal aspects visible. The left and right coracoids are preserved in dorsal view; both become wider and rectangular distally. The proximal ends are connected to the scapula, but the articulation at the glenoid fossa is poorly visible as it lies at the separation point between the main slab and main counterslab. The contact between the two bones has likely been deformed at least slightly by overburden compression. The left coracoid measures 40 mm long proximodistally, and 5.5 mm wide at the medial point. The right coracoid is better preserved, becoming wider distally 5 to 11 mm, with a defined tubercle on the medial side rimming an oblate depression. The left bone is fractured medially showing sponge-textured trabecular bone of the epiphysis. In close proximity lies a large, amorphous featureless plate-like bone, probably part of a sternum. The trunk is the least articulated area of the fossil, suggesting it collapsed before fossilisation, while most other elements remain preserved in *in-vivo* positions.

Both humeri are preserved; the right is seen from anterodorsal view, the left in anterior. The proximodistal length of the right humerus is 112 mm, and it is 35 mm and 20 mm wide at the proximal and distal ends of diaphysis, respectively. Thus, it is the largest Jurassic pterosaur humerus on record (the prior record-holder, to our knowledge, being the Early Jurassic isolated humerus NHMUK PV R36634, at 100 mm long, described by O'Sullivan[39]. The diaphysis is slender, measuring just 12 mm in width in the medial section, with a curve of 152°. The deltopectoral crest is lobate and proximally extending, diverging from the diaphysis at 134°, with a steep proximal articulation facet folding in at 109°, similar to the humeral morphology of *D. banthensis* (SNHM-2911-R[61]). The medial crest is large with a flat proximal region and steep contact with the diaphysis. There is a small tubercle on the diaphysis medially, possibly acting as the attachment of the triceps muscle. A similar tubercle is seen in the same position in *S. wucaiwanensis*. The distal articulation area is enlarged and globular. The supracondylar process is outstanding and curves anteriorly, almost perpendicular to the diaphysis, followed by a round ectepicondyle and entepicondyle, separated by a shallow trochlear depression. The left humerus is ~120 mm long as directly measured, with a diaphysis measuring 15-20 mm, curving at 170°. The discrepancy in length measurement compared to the right humerus may be due to localised flattening, expressed by visible fracturing on the bone surface. For this reason, we use the 112 mm length estimate from the better preserved right humerus for wingspan calculations. The deltopectoral area is preserved in three dimensions; the crest itself is split across the slabs. The deltopectoral crest flanks an oval depression housing the coracobrachialis muscle attachment.

Comparing humeri of pterosaurs is difficult, as these three-dimensionally complex bones with varying crests and processes usually preserve in two-dimensions at set of limited angles. The *Dearc* humerus is notably different from that of adult *Rhamphorhynchus*, which have a large rectangular protrusion set 90° from the diaphysis, or the shallow, rectangular deltopectoral crests of *Campylognathoides* and other basal Triassic pterosaurs. Humeri most similar to those of *Dearc* are found in non-pterodactyloids like of *D. banthensis* with a proximally inclined deltopectoral crest and flat proximal ulnar crest (especially seen in SMNS 50702).

Both ulnae are preserved in direct articulation with the humerus in dorsal view. The right ulna is 120 mm long, with an unchanging thickness of 10 mm. The right ulna is preserved alongside the diaphysis of the radius, which bears the same dimensions. Both ulna and radius are oval in cross-section (11 mm by 5 mm). The ulna has a lobate proximal tuberosity slotting into the lateral humeral trochlea. The left ulna is partially preserved, leaving a faint impression anterior to distal left humerus; the preserved element is 36 mm long, and 10 mm wide at the diaphysis.

No syncarpal bones, pteroid, or proximal metacarpals are preserved on either side of the animal. It is possible these elements were lost due to recent tidal erosion.

Both left and right fourth metacarpals (MCPIV) are present in the fossil. The right is seen from a posterior view, eroded to expose its medial cross-section (measurements in the bone wall section). The MCPIV is bordered by metacarpals I-III, which are tubular and circular in cross-section, bearing the same lengths and dimensions (2 mm by 2 mm). Distal articulation of the fourth metacarpal is obscured by the tri-lobate rugose extensor process of the first wing phalanx. The left MCPIV is seen in dorsoposterior view. The metacarpal is 45 mm long proximodistally, missing its distal syncarpal articulation. The proximal portion articulates with the robust wing phalanx I, with the extensor process sliding into the ginglymoid sulcus. The sulcus opens into a medial groove running down the length of the carpal body. The ginglymoid is bordered by hooked, laterally flat dorsal and ventral condyles of the same size (11 mm by 7 mm). The bone is oblate to lunate in the cross section.

The complete right manus is well preserved, retaining its three-dimensional topography. The manual phalanges do not change in thickness and terminate with rugose-textured condyles bordering the proximal articular facet, and the anterior ends have large triangular collateral ligament pits. The ungual claws have enlarged concave flexor tubercles. There are two antagonal sesamoids located above the ungual anterior crests of digit I and II. These are suggestive of enhanced grasping capabilities useful for an arboreal lifestyle[74]. The individual digits increase in length from digit I (24 mm), II (33 mm) to III (41 mm). The custom-made script by Cobb[75] was used to measure the internal and external curvature of the forelimb ungual. The inner curvature of claws measures within 70-90º; while the outer curvature measures within 90-130º, which in a bird reference dataset suggests a scansorial habitat[75]. The sesamoids have been observed in non-pterodactyloid pterosaurs[74], from basal *Dimorphodon macronyx* (NHMUK 41212) and *Dorygnathus banthensis* (BSP 1938 I) to derived *Kunpengopterus sinensis* (IVPP V 23674).

All wing phalanges are incomplete. The first wing phalanx (left) is preserved in lateroventral view, with a sizeable globular, rugose extensor process fused to the phalanx, acting as an attachment point for the m. flexor digiti quarti muscle. The phalanx has a deep medial groove opening from the proximal articulation point with the metacarpal intercondylar sulcus. How long the medial furrow extends is uncertain, as the distal phalanx aspect is crushed, obscuring details. The right wing phalanx is partially preserved, with the dorsal surface being only visible as an extensor process; this phalanx is eroded and displays a cross-section. The first wing phalanx (right) measures just 45 mm long proximodistally, 3-5 mm thick and is 4 mm deep. The second wing phalanx is preserved on the underside of the counter slab, belonging to the right wing; due to easy accessibility and existing fractures, this element was selected for histological sectioning. The diaphysis is straight with a smooth featureless texture and does not undulate in thickness. The third wing phalanx is preserved with a proximal articulation point, which has a straight margin, it retains some dorsoventral curvature (177º), although this might be affected by deformation.

Appendicular skeleton: pelvic girdle and hindlimbs

Sacral and pelvic elements in basal pterosaurs rarely preserve. This might be due to the region being small and composed of numerous thin elements prone to disarticulation in younger animals due to lack of ossification. The *Dearc* holotype exemplifies this. The pelvis is approximately 50 mm long, of which the sacral region makes half the total length. As the pelvis is preserved in ventral view, the ischium is represented as a cone-shaped amorphous plate. The right and left preacetabular processes are preserved; they are 32 mm long and 5 mm wide, with a slender shaft and a lobate proximal end. The right and left prepubis are preserved in articulation. The prepubis is hatchet shaped, 25 mm long with a width of 4 mm in the midsection and 16 mm at the proximal end. The prepubis lies close to 1 mm thin, long, interweaving elements, which composed the gastral basket. The proximal end of the femur is preserved and overlapped by the pubic plate. It has a “spoon” shaped proximal articulation. Just 30 mm of the bone is preserved, with a 4 mm wide shaft and 1 mm thick bone walls. The left set of metatarsals, not enclosed in tight-bundle, but splaying distally, are seen next to the mid-section of the caudal series. The terminal metatarsal is the thickest out of the bundle. No pedal digits and unguals are preserved, including the diagnostic digit V. No portions of the tibia or fibula are readily identifiable.

Bone histology, growth, and maturity

The wing phalanx of the *Dearc* holotype is well preserved and shows no signs of diagenetic alteration. The cortex is relatively thick, ranging from ~900–2400 µm, or 20–26% of the diameter of the bone. The cortex is composed entirely of primary fibrolamellar bone[76]. No

secondary remodelling is present within the cortex, but a thin layer of endosteal lamellar bone surrounds the medullary cavity. A prominent line of arrested growth (LAG) is present on one side of the cortex, but is intersected by the medullary cavity, providing evidence of cortical drift. A second LAG is present in most regions about 20–30 µm internal to the periosteal surface. The fibrolamellar cortex is highly vascularized throughout, and vascularity is predominantly reticular in orientation, with a relatively high proportion of radial canals. No significant variation in vascular density or orientation can be observed, either between regions of the cortex or within zones demarcated by LAGs. However, few vascular canals can be observed external to the second LAG where it is present. It is unclear whether this represents deposition of more poorly vascularized bone, or whether there is simply not enough bone deposited to have embedded many vascular canals: the 20–30 µm rind of bone is far narrower than the spacing between vascular canals in the rest of the cortex. The bone external to the second LAG has a parallel-fibered matrix, indicative of slower growth than the rest of the cortex. A similar thin zone of parallel-fibered bone is present just external to the more internal LAG. In the regions where the second LAG is absent, vasculature reaches the periosteal surface, but few of the canals communicate with the periosteal surface. Vascular canals throughout are small in diameter and are surrounded by thin layers of lamellar bone. Thus, the fibrolamellar bone of the cortex appears to be composed of a high proportion of woven-fibered bone. Osteocyte lacunae are small and relatively dense (~50,000/mm^3).

Maturity—The presence of two LAGs in the cortex of the *Dearc* holotype indicate a minimum age of 2 years, although it is possible that the specimen is older and some growth marks have been erased by cortical drift or expansion of the medullary cavity. The position of the second LAG close to the external surface of the bone suggests that the individual perished shortly after emerging from its growth hiatus. The highly vascularized, woven cortical bone of the *Dearc* holotype indicates a rapid rate of growth[13]. The presence of dense vasculature extending to the external surface of the bone and the absence of a well-defined external fundamental system indicate that this individual was still actively growing when it perished[77]. The 20–30 µm-thick zone of parallel-fibered bone at the periosteal surface may indicate that the growth rate of the individual was decreasing[13], but this is ambiguous. A similar thin zone of parallel-fibered bone is present external to the first LAG, which indicates a gradual increase in growth rate after the seasonal growth hiatus. Thus, it is possible that the parallel-fibered bone at the periosteal surface is not an indicator of decreased growth rate, but rather that the individual was gradually emerging from its growth hiatus when it died. Regardless, the absence of this zone of parallel-fibered bone around the entire external surface and the absence of an external fundamental system or any slow-growing lamellar bone mean that this individual is best considered an actively growing juvenile–subadult.

If the zone of parallel-fibered bone at the periosteal surface does reflect a decrease in growth rate, which might be tested by future sampling of other parts of the skeleton, it may indicate that the individual had reached sexual maturity, as this typically results in a decrease in growth rate as energy is diverted from growth towards reproduction[78]. Prondvai et al.[14] proposed an alternative explanation for decreasing growth rates observed in their sample of *Rhamphorhynchus*, extrapolating to other pterosaurs: the onset of powered flight. However, this seems unlikely to be the case based on the large size and wingspan of *Dearc*, which nonetheless shows no evidence of a decrease in growth rate. It is difficult to reconcile the large wingspan of *Dearc* with a non-volant or arboreal lifestyle, and instead it seems more reasonable to infer that this large animal was capable of flying despite continuing to actively grow. Thus, we infer that the transition to slower growth after several years in *Rhamphorhynchus* and other pterosaurs is more likely to correspond with sexual maturity, as it does in nearly all vertebrates that reach sexual maturity after more than one year of age[79]. This conclusion is likewise supported by the recent finding of isometry in

Rhamphorhynchus[19], and evidence for flight in other hatchling pterosaurs[80]. In any case, it is clear that the holotype of *Dearc* had not yet reached maximum body size, and if it had reached sexual maturity, it was only just before it perished.

Comparative histology

Histological studies of non-pterodactyloid bone material have become more common, and bone microstructure is now known from a number of non-pterodactyloids spanning the early phases of pterosaur evolution. These include Late Triassic basal non-pterodactyloids (MGUH VP 3393[16]), the Early Jurassic *Dorygnathus*[81] and *Dimorphodon*[16, 82], an ontogenetic sequence from the Late Jurassic *Rhamphorhynchus*[14, 16], and isolated elements from Tayton Limestone[82, 83], roughly coeval to our Scottish specimen. Comparison of the histology of *Dearc* with previous studies on pterosaur histology provides further evidence to support the interpretation of its growth rate and maturity.

In general, most pterosaur histological sections, including those of non-pterodactyloids, indicate a pattern of rapid growth early in life, more similar to that of mammals, non-avian dinosaurs, and birds, rather than slower growth exhibited by squamates[16]. Padian et al. (2004)[16] noted some minor variations in tissue type and inferred growth rates between smaller and larger species, wherein smaller species tended to grow at slower rates, a phenomenon also recognized in non-avian dinosaurs[84]. In contrast, smaller specimens within a single species tend to exhibit higher proportions of densely vascularized fibrolamellar bone[14], which represents relatively fast bone deposition early in life. In some larger specimens, the cortex preserves a progressive decrease in vascularity and an increased proportion of parallel-fibered bone, recording a decrease in growth rate[14] that likely corresponds to the achievement of sexual maturity (see above). The largest specimens within a species tend to exhibit strongly remodelled cortices of poorly vascularized parallel-fibered bone, indicative of advanced ontogenetic age, low growth rates, and terminal growth stages [14, 85, 86]. However, this broad pattern, shared with non-avian dinosaurs and mammals, can be complicated both by variation between skeletal elements of the same individual, and by significant developmental plasticity, such that size is a poor predictor of histological maturity in some taxa, especially in the middle size classes[14,86]. Analyses of pterosaur growth are further complicated by the thin-walled bones of pterosaurs[80], which are maintained by extensive expansion of the medullary cavity and considerable cortical drift, processes that erase the early record of growth. Thus, in pterosaurs it is difficult to assess skeletochronology using lines of arrested growth, or to assess differences in growth patterns between species from non-overlapping material.

In this light, two comprehensive analyses of non-pterodactyloid palaeohistology are critical for evaluating growth and maturity in *Dearc*: the studies of Padian et al. (2004)[16] and Prondvai et al. (2012)[14]. Whereas Padian et al. (2004) examined multiple species showing generally conserved growth patterns in the clade, Prondvai et al. (2012)[14] examined an ontogenetic series of *Rhamphorhynchus*, which provides a useful baseline for interpreting the relative maturity of the closely related *Dearc*. The Prondvai et al. (2012)[14] study examined multiple bones from five individuals and analyzed their growth and maturity in light of their estimated body sizes. The results suggested three age classes could be distinguished based on histology (but not always size): (1) hatchlings/early juveniles, characterized by fast-growing fibrolamellar bone tissues, dense vascularity, and large osteocyte lacunae; (2) late juveniles/subadults showing a decrease in growth rate towards the external cortex marked by parallel-fibered bone, and tending to exhibit one or more annuli or LAGs; and (3) adults, which exhibit slow growth (although no external fundamental systems were present in their sample), and secondary remodelling. Under this framework, the wing phalanx of *Dearc* falls somewhere between stage 1 and 2, because its cortex is formed exclusively of fibrolamellar

bone that does not yet exhibit any evidence of decreased growth, but it does exhibit lines of arrested growth. This is interesting considering the size of the holotype, as Prondvai et al. (2012)[14] found that individuals of *Rhamphorhynchus* exhibited evidence for decreased growth rate by the time they had reached 30–50% of adult wingspan. Although it is unknown how broadly this figure applies across non-pterodactyloid pterosaurs, if *Dearc* had a life history similar to the closely-related *Rhamphorhynchus*, it would indicate that fully-grown individuals were much larger—possibly ca. 7.512 meters in wingspan, if we take the 3.76 m wingspan estimate for the *Dearc* holotype based on *Rhamphorhynchus* humerus scaling and double it (assuming the individual was 50% adult wingspan). Such a large wingspan seems implausible, but this exercise demonstrates that, based on all comparisons to closely related *Rhamphorhynchus* (humerus and skull scaling equations, histology), *Dearc* was a much larger pterosaur.

The wing phalanx of the holotype of *Dearc* is histologically consistent with other pterosaur wing phalanges presently known, and wing phalanges are generally considered useful indicators of overall growth in pterosaurs[14, 16, 82, 85, 86]. For example, the wing phalanx of *Dearc* is similar to the third wing phalanx of *Rhamphorhynchus* described by Prondvai et al. (2012)[14] in that it exhibits an outer cortex of fibrolamellar bone with one LAG, and endosteal lamellae providing evidence of medullary expansion. However, *Dearc* differs from this individual of *Rhamphorhynchus* in that the inner cortex is not remodelled by secondary osteons, a process expected to progress with increasing age. Padian et al. (2004)[16] described the wing phalanges of *Rhamphorhynchus* and *Pterodactylus*, which differed significantly in microstructure. Whereas the wing phalanx of *Rhamphorhynchus*, representing a relatively large individual, showed reduced vascularity and two LAGs, that of *Pterodactylus* was densely vascularized and lacking LAGs or evidence of decreasing growth, despite being similar in size to the large *Rhamphorhynchus* individual. In these respects, the holotype of *Dearc* is more similar to *Pterodactylus*, as it is heavily vascularized and shows no evidence for decreasing growth, despite the presence of two LAGs.

However, in some ways, the histology of the wing phalanx of *Dearc* more closely resembles growth patterns described in pterydactyloids. For example, it is similar in terms of vascular density and orientation, cortical thickness, and the presence of LAGs to the internal cortices of the wing phalanges of *Montanazhdarcho* and *Pteranodon*[86]. Likewise, it is similar in bone texture to a Late Jurassic dsungaripteroid femur (SHN.013), belonging to an animal of approximately the same large estimated wingspan[87]. However, it has fewer circumferential vascular canals than SHN.013 and lacks the external fundamental system preserved in this specimen. The wing phalanx of *Dearc* is also similar in the dominance of fibrolamellar bone and dense vascularity to juvenile *Hamipterus* ulnae[15], although the plexiform arrangement of the vasculature in those individuals indicates more rapid bone apposition than in *Dearc*, possibly as a result of the different elements analyzed. The *Hamipterus* individuals, spanning ontogeny for this species, show evidence of decreasing growth towards the periosteal surface with increasing size. A transition towards the outer cortex provides evidence for sexual maturity in the largest individuals[15], but this transition only appears after the ulna had reached ~70% of the linear dimensions of the largest individual.

Overall, comparison of the histology of the wing phalanx of *Dearc* with other pterosaurs supports the idea that it was a rapidly growing individual and would have attained a larger size as an adult. The density of vasculature and its arrangement is more similar to larger-bodied pterosaurs, especially pterodactyloids, supporting the idea that it was a large-bodied taxon. Furthermore, the distribution of tissues within the cortex and the absence of evidence for a decreased growth rate towards the end of life support the conclusion that it was at an early ontogenetic stage. Comparisons to other pterosaurs where several ontogenetic stages are documented[14,15] suggests that the holotype of *Dearc* may have grown considerably

larger as an adult, as the transition to sexual maturity is reached between 30–50% of adult wingspan in the non-pterydactyloid *Rhamphorhynchus*[14], and approximately 70% of adult size in *Hamipterus*[15]. Despite an estimated wingspan of 1.9-3.8 meters based on regression equation used, the holotype of *Dearc* had apparently not yet reached such a late stage of life, and thus its full adult size.

Figure

Click here to access/download;Figure;Fig1.png

Figure

Click here to access/download;Figure;Fig2.png

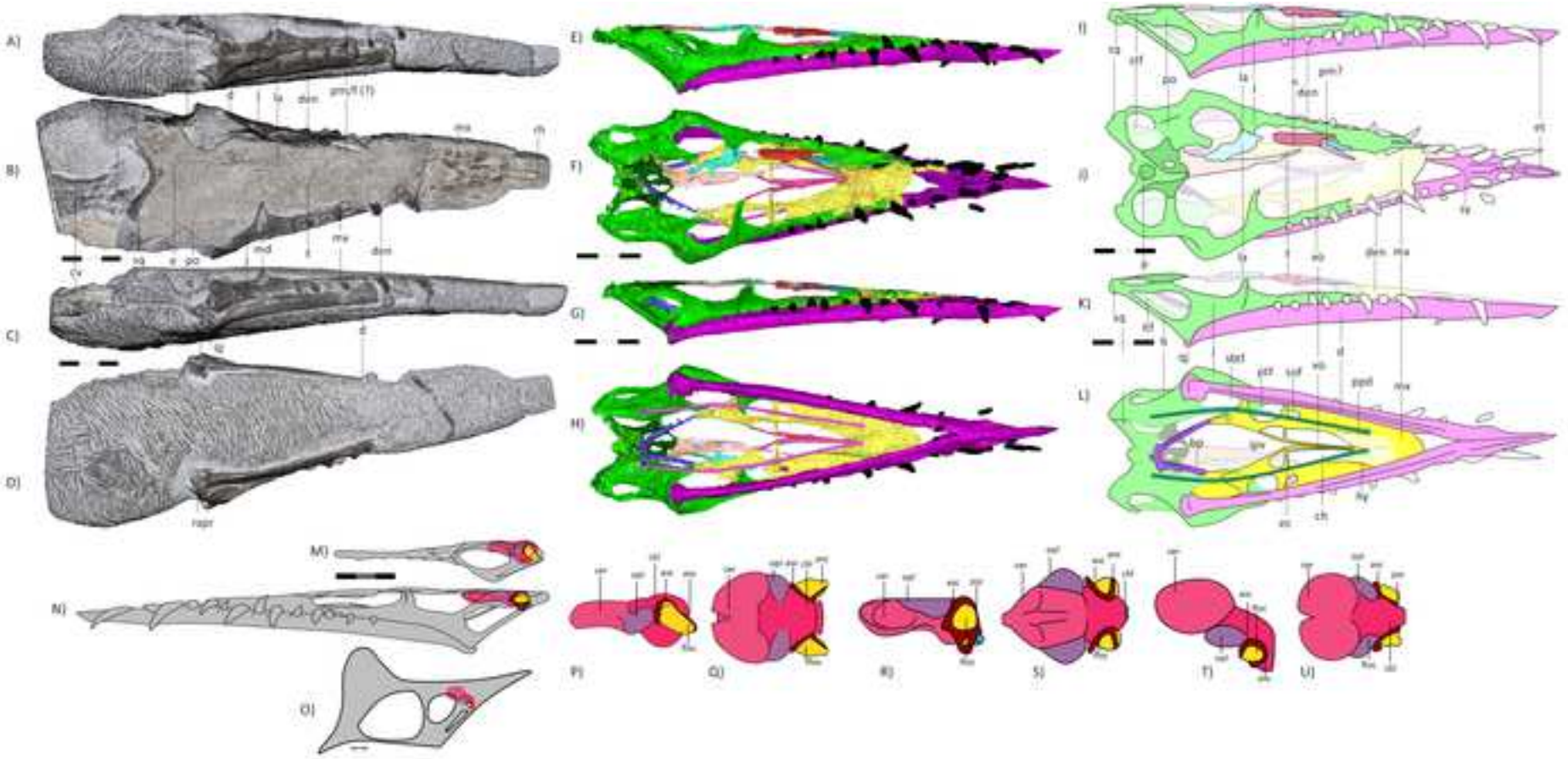

Figure

Click here to access/download;Figure;Fig3.png

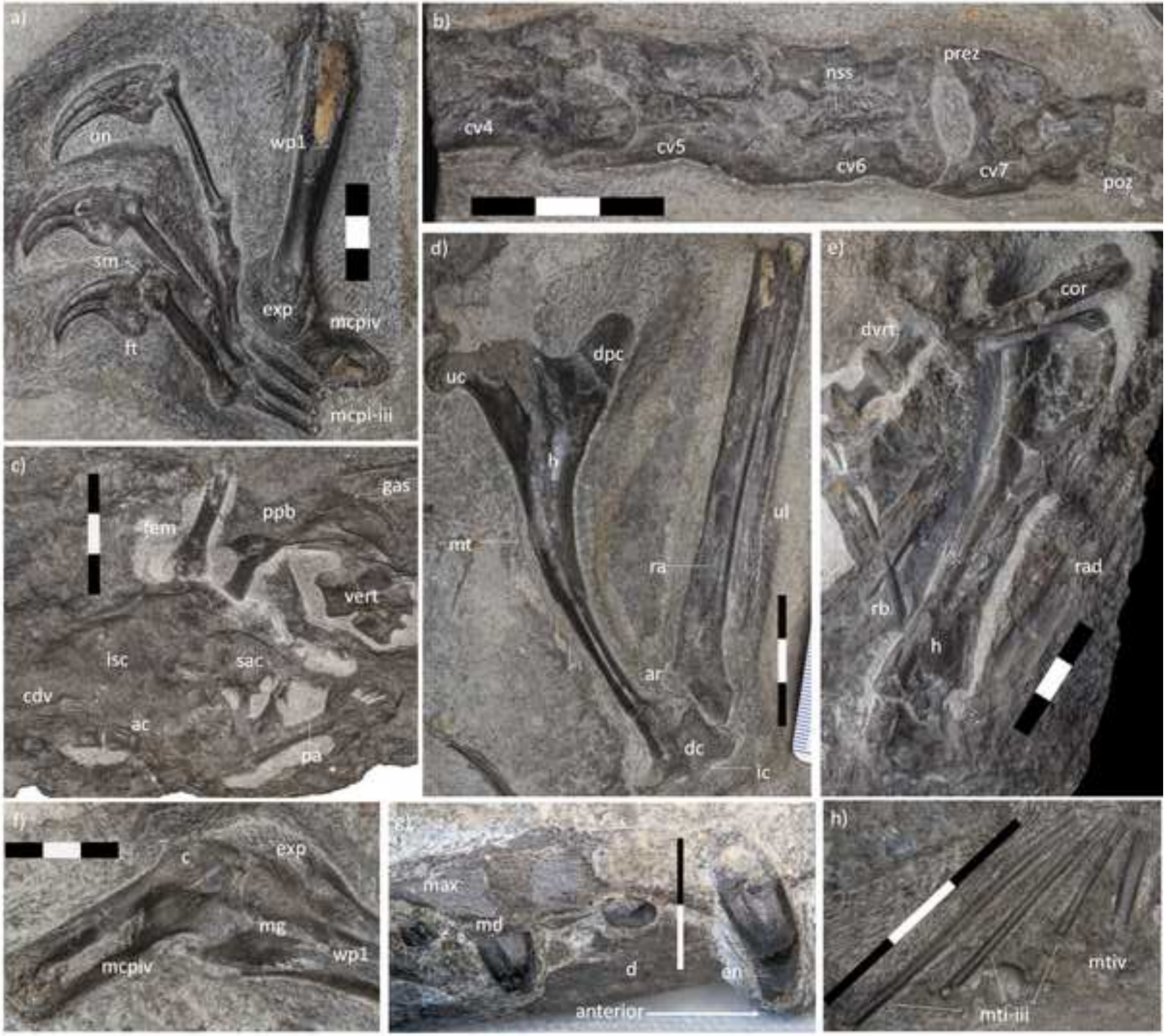

Figure

Click here to access/download;Figure;Fig4.png

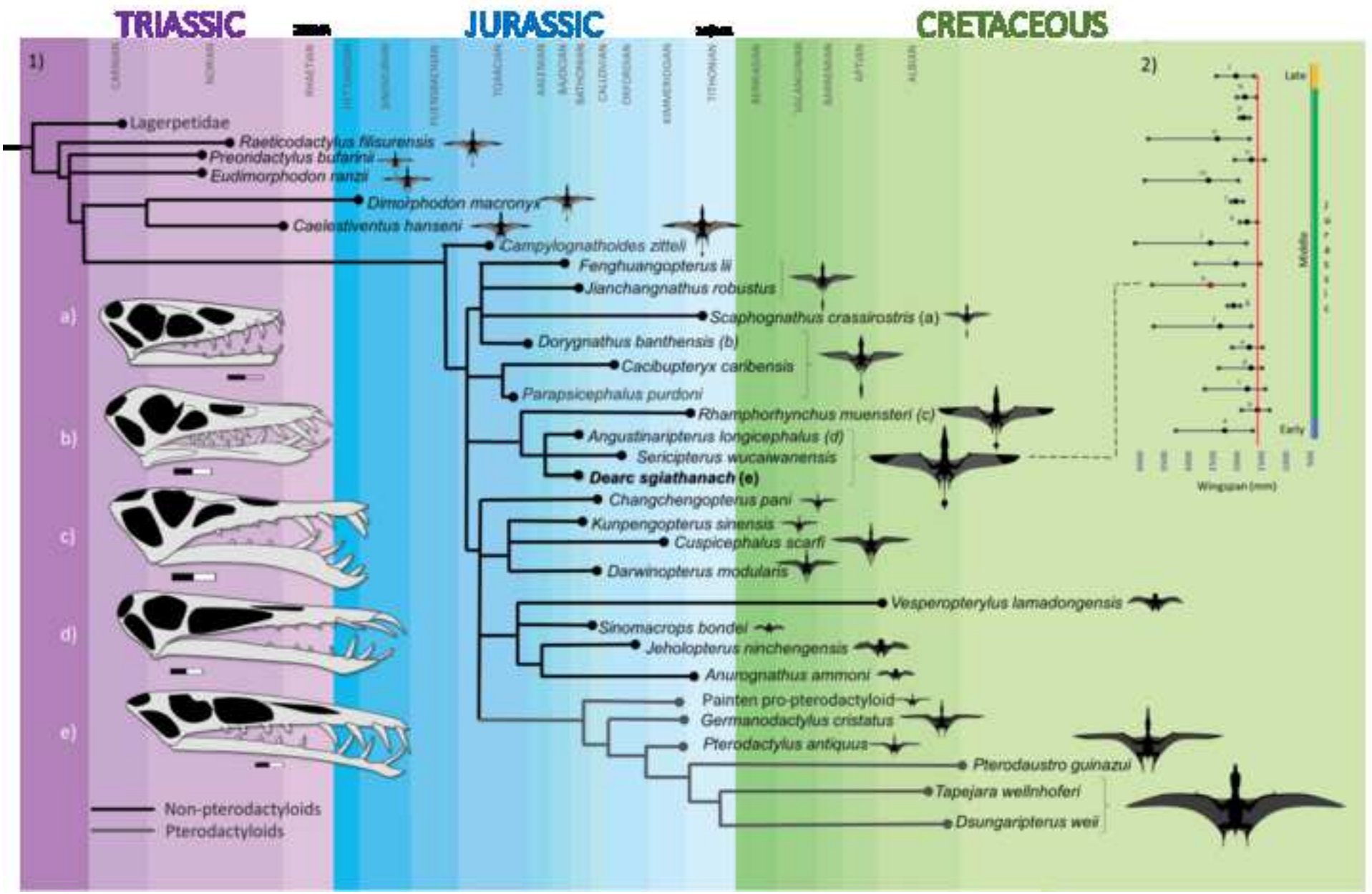

Additional Supplementary Files

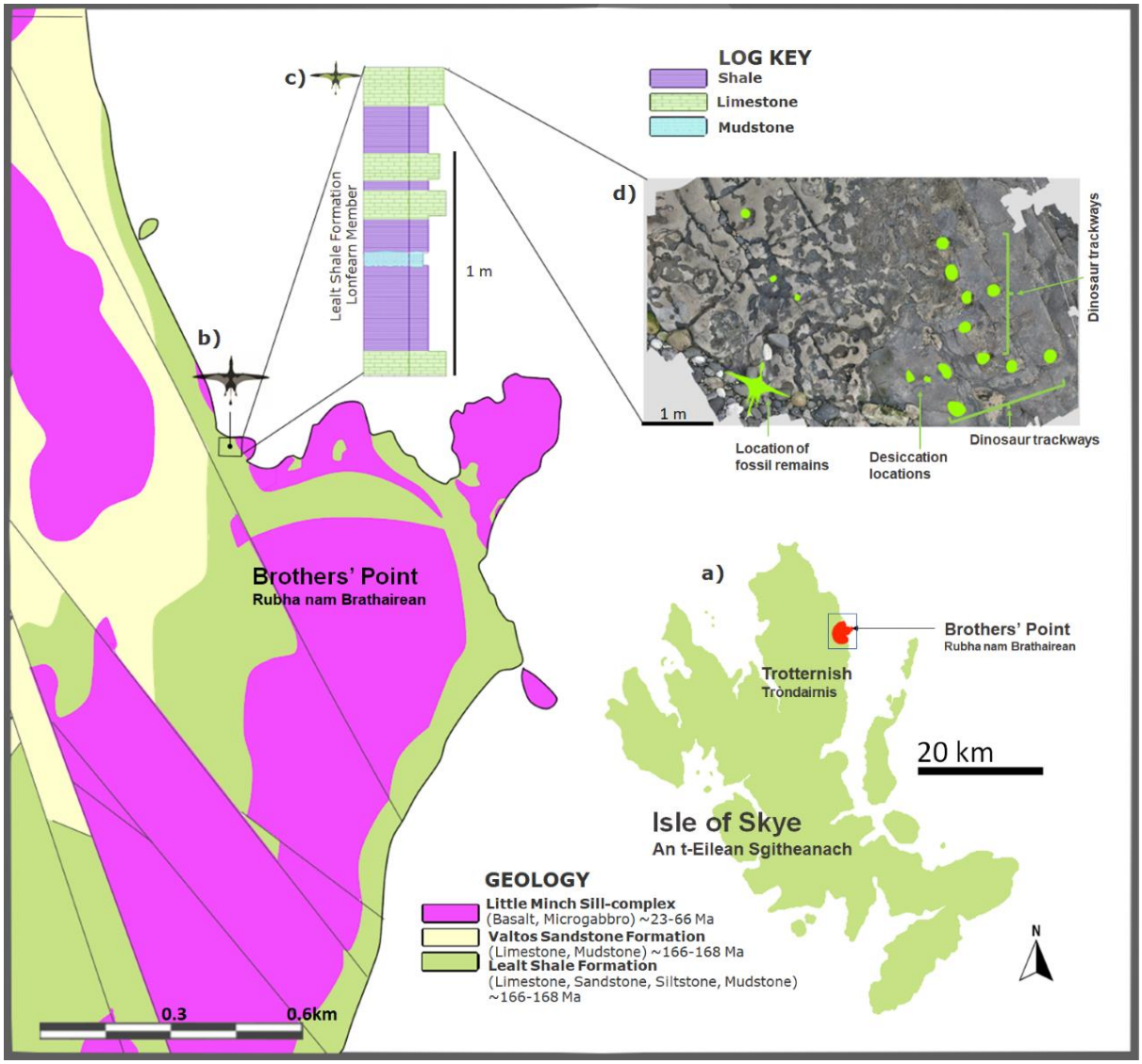

Figure 1. Locality information for the holotype of the new Middle Jurassic pterosaur *Dearc sgiathanach*. Map and geological context showing: Isle of Skye (a); geological map of the locality where the specimen was found, Brothers' Point (b); stratigraphic section at the discovery site (c); orthophoto of the pterosaur fossil location in relation to dinosaur trackways and evidence of desiccation (d). Figures c) & d) modified after dePolo et al. (2020).

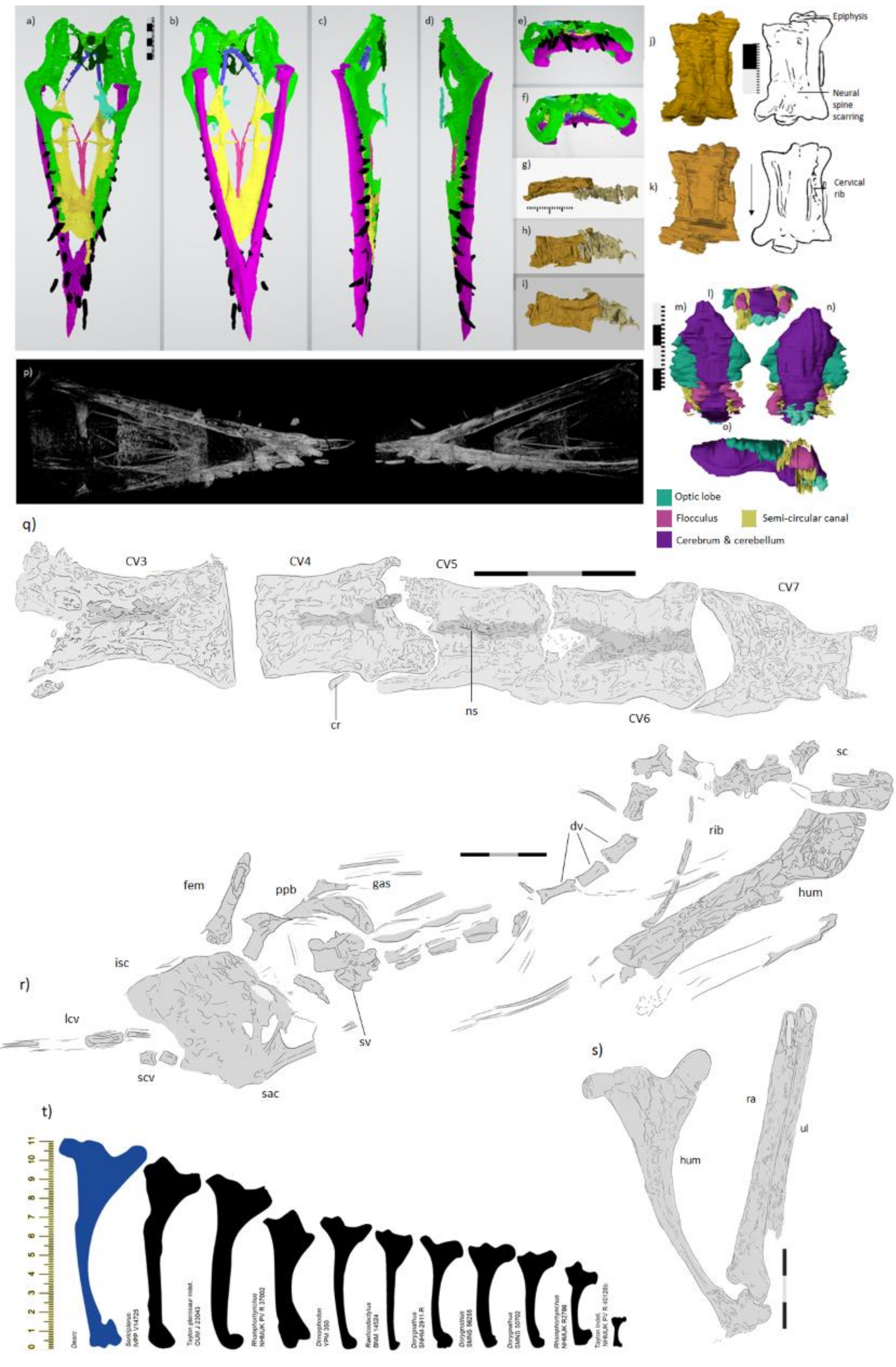
a)
b)
c)
d)
e)
f)
g)
h)
i)
j)
Epiphysis
Neural spine scarring
k)
Cervical rib
l)
m)
n)
o)
Optic lobe
Flocculus
Semi-circular canal
Cerebrum & cerebellum
p)
q)
CV3
CV4
CV5
CV6
CV7
cr
ns
r)
sc
dv
rib
hum
fem
ppb
gas
isc
lcv
scv
sac
sv
s)
ra
ul
hum
t)
Dearc
Sericipterus IVPP V14725
Tayton plesiosaur indet. OUM J 23043
Rhamphorhynchus NHMUK PV R 37002
Dimorphodon YPM 350
Raeticodactylus BNM 14524
Dorygnathus SMNS 50702
Rhamphorhynchus NHMUK R2786
Tayton indet. NHMUK PV R 40126b

Fig. 2. Skull and anterior cervical vertebrae of the new Middle Jurassic pterosaur *Dearc sgiathanach* visualised by X-ray computed microtomography (manual & machine learning segmentation). Manually segmented skull in: (a) dorsal; (b) ventral; (c) right lateral; (d) left lateral; (e) anterior; (f) posterior views. Colour code: yellow – palate & pterygoid; purple – dentary; black – teeth; green – fused dorsal cranial elements; blue – basipterygoid; light blue – dorsal unfused cranial bones. Manually segmented atlas, axis & anterior cervical complex in: (g) lateral; (h) ventral; (i) dorsal views. Cervical close up with schematic line art in: (j) dorsal and (k) ventral views. Colour code: dark yellow – 3rd cervical; cream – atlas & axis. Manually segmented brain and inner ear endocast in: (l) anterior; (m) dorsal; (n) ventral; (o) left lateral views. Colour code [annotated in the figure] channels; dark blue – optic lobes; pink – flocculus; purple – cerebrum & cerebellum; light blue – cranial nerves; WEKA trained machine learning segmentation results (p) in dorsal and ventral (left to right, respectively). Line art of select elements (q) cervical vertebral series in dorsal view, abbreviations: cv# - cervical vertebra; cr - cervical ribs; ns - neural spine; NMS G.2021.6.3 counterslab (r) in ventral orientation, abbreviations: lcv - long caudal vertebra; scv - short caudal vertebra; isc - ischium; ppb - prepubis; sv - sacral vertebra (?); gas - gastralia; sac - sacrum; dv - dorsal vertebra; rib - dorsal ribs; hum - humerus; sc - scapula coracoid; and dorsal view of right humerus (s); abbreviations: hum - humerus; ra -radius; ul - ulna. Comparative size diagram of select non-pterodactyloid humeri (t) [annotated in image]. Scales bars=20 m

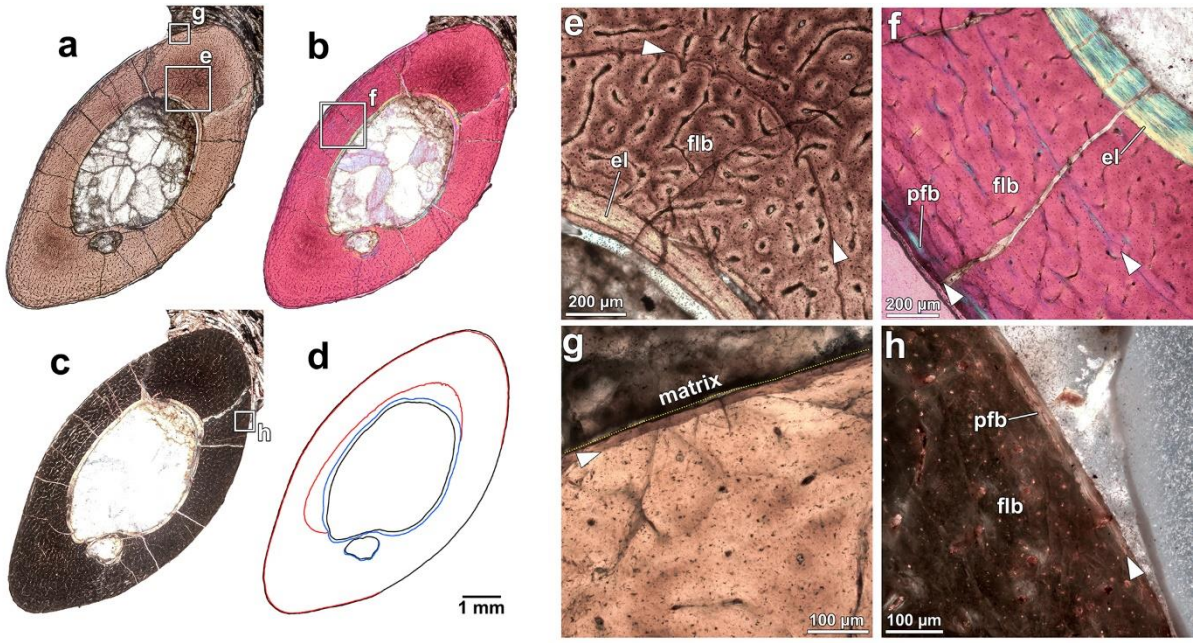

Fig. 3. Histology of the wing phalanx of the new Middle Jurassic pterosaur *Dearc sgiathanach*. Thin section in plane polarized light (a), cross-polarized light with a lambda filter (b), cross-polarized light (c), and illustration (d) of histological features: lines of arrested growth (red) and endosteal resorption (blue). Note position of external line of arrested growth very close to the external surface. (e) Inner cortex of wing phalanx under plane polarized light, showing densely vascularized fibrolamellar bone with a line of arrested growth (arrows). (f) Cortex of wing phalanx under cross-polarized light with a lambda filter, showing endosteal lamellae (el), lines of arrested growth (arrows), predominance of primary fibrolamellar bone (flb), and an external zone of parallel-fibered bone (pfb). Note parallel-fibered bone (appearing cyan) adjacent to the line of arrested growth. (g) External cortex of wing phalanx under plane polarized light, showing line of arrested growth (arrow) adjacent to the external bone surface (below dotted yellow line). (h) External cortex of wing phalanx under cross-polarized light, showing parallel-fibered bone (pfb) at the periosteal surface, possibly indicating a decrease in growth rate from the earlier fibrolamellar bone (flb). Arrows denote lines of arrested growth. **Abbreviations**: **el**, endosteal lamellae; **flb**, fibrolamellar bone; **pfb**, parallel-fibered bone.

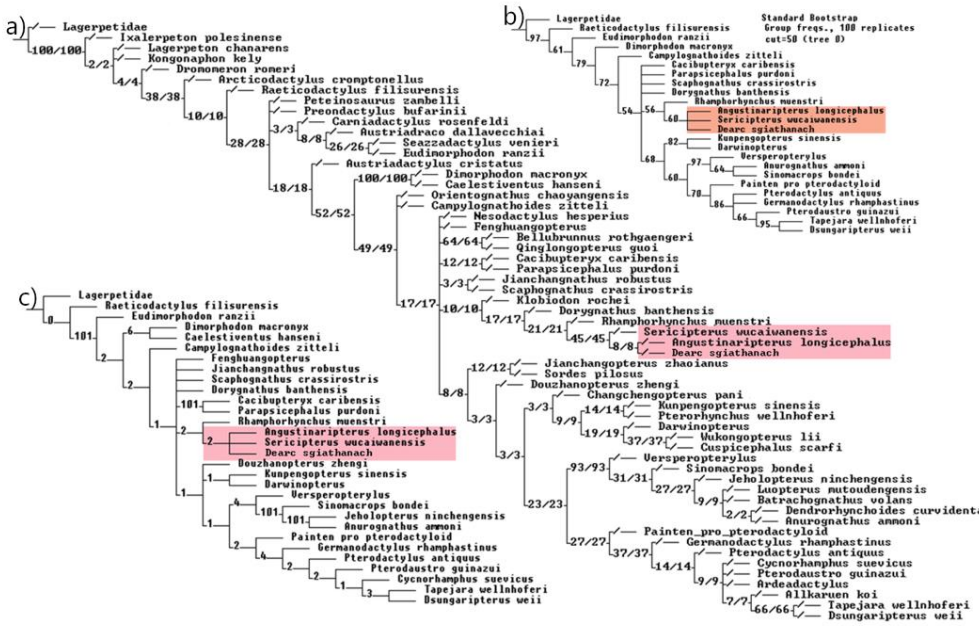

Fig. 4. Results of phylogenetic analysis of the relationships of *Dearc sgiathanach* and other basal pterosaurs: (a) Bootstrap Frequency difference (GC) tree without wildcard or problematic taxa removal from consensus (GC, 100 replicates); (b) Bootstrap absolute frequency tree with problematic taxa removed; (c) Bremer support values, (Bremer.run) with removal of problematic taxa. In each, the red box denotes the clade Angustinaripterini.

Details of Phylogenetic Analysis

Outgroups

Ixalerpeton polesinense (ULBRA-PVT059)
Kongonaphon kely (UA 10618)
Lagerpeton chanarens (MCZ 10154; PVL 462; PVL 4619; PULR 06)
Dromomeron romeri (GR 238/222/218/223; TMM 31100-1334)
In the consensus tree the four terminal taxa were combined together to form a composite **Lagerpetidae** terminal group, as no individual lagerpetid is near complete enough to act as a reasonable outgroup taxon.

Triassic basal non-pterodactyloids

Raeticodactylus filisurensis (BNM 14524)
Preondactylus bufarinii (MCSNB 4562, MFSN 1770, MFSN 25161)
Caelestiventus hanseni (BYU 20707)
Eudimorphodon ranzii (MCSNB 2888 (holotype), BSP 1994I 51)

Pterosaurs included in original search but removed from consensus, with rationale for removal:

Carniadactylus rosenfeldi (MFSN 1797) – here treated as co-generic with *Caviramus schesaplanensi*
Seazzadactylus venieri (MFSN 21545) – partial material
Arcticodactylus cromptonellus (NHMD74799) – on degree of lack of completion, immaturity
Bergamodactylus wildi (MPUM 6009) – on questionable ontogenetic affinity
Austriadraco dallavecchiai (BSP 1994 I 51) – limited material
Austriadactylus cristatus (SMNS 56342, SC 332466) – poor, deformed incomplete material
Peteinosaurus zambelli (MCSNB 2886; MCSNB 3496) – elements too heavily overlapped

Jurassic non-pterodactyloids

Rhamphorhynchus muenstri (NHMUK PVOR37002; Goldfuss, 1831/ MTMV 2008.33.1; TMP 2008.41.001; YPM 1178; Dark Wing; Zittel Wing; CM 1143; JME-SOS4009; CM 11427; and other specimens noted in Wellnhofer (1975))
Dorygnathus banthensis (Specimens as described by Padian, 2008)
Scaphognathus crassirostris (Goldfuss, 1831 holotype; SMNS 59395)
Campylognathoides zitteli (as described by Padian, 2008)
Cacibupteryx caribensis (IGO-V 208, holotype)
Angustinaripterus longicephalus (ZDM T8001, holotype)
Jianchangnathus robustus (IVPP V16866/PMOL-AP00028)
Sordes pilosus (PIN 2585/3; PIN 2470/1; PIN 2585/25; PIN 2585/4a)
Dimorphodon macronyx (NHMUK R1035/41212)
Parapsicephalus purdoni (GSM 3166, holotype)
Sericipterus wucaiwanensis (IVPP V14725 holotype)
Fenghuangopteruslii (CYGB-0037; BMNHC PH000988)

Jurassic Wukongopterids

Darwinopterus sp. (IVPP V16049, HGM 41HIII-0309A, ZMNH M8802, ZMNH M8782, IVPP V16049)
Kunpengopterus sinensis (IVPP V 23674, IVPP V 16047, IVPP V 17959)
Cuspicephalus scarfi (MJML K1918)

Changchengopterus pani (PMOL-AP00010)
Wukongopterus lii (IVPP V15113)

Jurassic Pterosaurs included in original searches but removed, with rationale for removal:

Rhamphorhynchus etchesi (MJMLK-1597) – incomplete
Orientognathus chaoyngensis (HGM 41HIII-0418) – immature
Campylognathoides liascus (Padian, 2008... on assumption of immature *C. zitteli*)
Nesodactylus hesperius (AMNH 2000) – incomplete
Jianchangopterus zhaoianus (YHK-0931, holotype) – now recognised as immature wukongopterid
Qinglongopterus guoi (D3080/1) – immature
Bellubrunnus rothgaengeri (BSP-1993-XVIII-2) – immature
Klobiodon rochei (NHMUK PV OR 47991, holotype) – too incomplete
Harpactognathus gentryii (NAMAL 101) – too incomplete (removed from matrix)
Pterorhynchus wellnhoferi – lack of specimen access/inaccessible resources
Allkaruen koi (MPEF-PV 3613) – too incomplete, modular nature led to polytomy
*Douzhanopterus zhengi (*STM 19–35A & B) – immature

Anurognathids

Anurognathus ammoni (BSPG 1922.1.42; SMNS 81928a/b)
Jeholopterus ninchengensis (IVPP V12705; CAGS-IG-02-81)
Sinomacrops bondei (JZMP-2012-001)
**Luopterus mutoudengensis* (JZMP-04-07-3)
**Dendrorhynchoides curvidentatus* (GMV 2128)
**Batrachognathus volans* (PIN 52-2; PIN 2585/4a)
Versperopterylus ninchengensis (BMNHC-PH-001311)

As there is no sound way of assessing taxonomic relationships of this group, due to variance in preservation and ontogeny, the group has been reduced to 3 taxa (removed marked with asterisk), as in preliminary runs of our analysis their lack of distinctive features resulted in a large unresolved polytomy.

Jurassic Pterodactyloids

*Pterodactylus antiquus (*AMNH 1942; BSP AS V 29; MB.R. 3530 (14); 3533 (3); BSP 1883 XVI 1; BSP 1929 I 18; Collini holotype - BSP AS I 739 and specimens as illustrated by Wellnhofer, 1970)
Painten pro-pterodactyloid (Tischlinger, 2013)
Cycnorhamphus suevicus (GPIT 80)
*Germanodactylus rhamphastinus (*BSP 1892 IV 1; "BSP AS I 745a/b")
Ardeadactylus longicollum (SMNS 56603 & lost holotype)

Derived pterodactyloids

Tapejara wellnhoferi (AMNH 24440; SMNK PAL 3986; SMNK PAL 1133; SMNK PAL 1137)
Dsungaripterus weii (IVPP V 4063; IVPP V4065; IVPP V 26256; IVPP V 2776; IVPP V 26560; IVPP V 26257; IVPP V 26259; IVPP V 26258; V4063 from Junchang, 1997)
Pterodaustro guinazui (MMP 1018; MMP 3562; MIC-V263)

Phylogenetic characters from:

- Andres, B. and Myers, T.S., 2012. Lone star pterosaurs. *Earth and Environmental Science Transactions of the Royal Society of Edinburgh*, *103*(3-4), pp.383-398.
- Andres, B., Clark, J. and Xu, X., 2014. The earliest pterodactyloid and the origin of the group. *Current Biology*, *24*(9), pp.1011-1016.
- Britt, B.B., Dalla Vecchia, F.M., Chure, D.J., Engelmann, G.F., Whiting, M.F. and Scheetz, R.D., 2018. Caelestiventus hanseni gen. et sp. nov. extends the desert-dwelling pterosaur record back 65 million years. *Nature ecology & evolution*, *2*(9), pp.1386-1392.
- Dalla Vecchia, F.M., 2009. Anatomy and systematics of the pterosaur Carniadactylus gen. n. rosenfeldi (Dalla Vecchia, 1995). *Rivista Italiana di Paleontologia e stratigrafia*, *115*(2), pp.159-188.
- Dalla Vecchia, F.M., 2019. Seazzadactylus venieri gen. et sp. nov., a new pterosaur (Diapsida: Pterosauria) from the Upper Triassic (Norian) of northeastern Italy. *PeerJ*, *7*, p.e7363.
- Kammerer, C.F., Nesbitt, S.J., Flynn, J.J., Ranivoharimanana, L. and Wyss, A.R., 2020. A tiny ornithodiran archosaur from the Triassic of Madagascar and the role of miniaturization in dinosaur and pterosaur ancestry. *Proceedings of the National Academy of Sciences*, *117*(30), pp.17932-17936.
- Kellner, A.W., 2003. Pterosaur phylogeny and comments on the evolutionary history of the group. *Geological Society, London, Special Publications*, *217*(1), pp.105-137.
- Lu, J. and Ji, Q., 2006. Preliminary results of a phylogenetic analysis of the pterosaurs from western Liaoning and surrounding areas. *JOURNAL-PALEONTOLOGICAL SOCIETY OF KOREA*, *22*(1), p.239.
- Unwin, D.M., 2003. On the phylogeny and evolutionary history of pterosaurs. *Geological Society, London, Special Publications*, *217*(1), pp.139-190.
- Vidovic, S.U. and Martill, D.M., 2014. Pterodactylus scolopaciceps Meyer, 1860 (Pterosauria, Pterodactyloidea) from the Upper Jurassic of Bavaria, Germany: the problem of cryptic pterosaur taxa in early ontogeny. *PloS one*, *9*(10), p.e110646.
- Vidovic, S.U., 2016. A Discourse on Pterosaur Phylogeny (Doctoral dissertation, University of Portsmouth).
- Wang, X., Kellner, A.W., Jiang, S. and Meng, X., 2009. An unusual long-tailed pterosaur with elongated neck from western Liaoning of China. *Anais da Academia Brasileira de Ciências*, *81*, pp.793-812.

Terminal taxa excluded from strict consensus in Figure 4.1

Cycnorhamphus suevicus; Luopterus mutoudengensis; Dendrorhynchoides curvidentatus; Batrachognathus volans; Orientognathus chaoyngensis ; Campylognathoides liascus; Nesodactylus hesperius; Jianchangopterus zhaoianus; Qinglongopterus guoi; Bellubrunnus rothgaengeri; Klobiodon rochei; Pterorhynchus wellnhoferi; Allkaruen koi; Douzhanopterus zhengi; Wukongopterus lii; *Sordes pilosus; Ixalerpeton polesinense; Kongonaphon kely; Lagerpeton chanarens; Dromomeron romeri; Carniadactylus rosenfeldi; Seazzadactylus venieri ; Arcticodactylus cromptonellus; Bergamodactylus wildi; Austriadraco dallavecchiai; Austriadactylus cristatus; Peteinosaurus zambelli*

Institutional Abbreviations:

AMNH, American Natural History Museum, US
BMNHC, Beijing Museum of Natural History, Beijing, China
BNM, Bündner Naturmuseum, Chur, Switzerland
BSP, Bayerische Staatssammlung für Paläontologie und Geologie, Munich (Germany)
BSPG, Bavarian State Collection for Palaeontology, Munich, Germany
BYU, Museum of Paleontology, Brigham Young University, Provo (USA)
CAGS, Chinese Academy of Geological Sciences, Beijing, China
CCMGE, Chernyshev's Central Museum of Geological Exploration, Saint Petersburg, Russia
CM, Carnegie Museum of Natural History, Pittsburgh, Pennsylvania, USA

CYGB, Chaoyang Bird Fossil National Geopark, China
DM, Dinosaur Museum, Blanding, Utah, USA
FHSM, Sternberg Museum of Natural History, Hays, KS, USA
GMV, Geological Museum of China, Beijing, China
GPIT, Geologisch-Paliiontologisches Institut, Tiibingen
GR, Ghost Ranch Ruth Hall Museum of Paleontology, Ghost Ranch, New Mexico, USA;
GSM, British Geological Survey, UK
HGM, Henan Geological Museum, Zhengzhou, Henan Province
IGO, Museo Mario SaÂnchez Roig, Instituto de GeologõÂa y PaleontologõÂa, La Habana, Cuba
IVPP, Institute of Vertebrate Paleontology and Paleoanthropology, Beijing, China
JME, Jura Museum, Eichstätt, Germany
JZMP, Jinzhou Paleontological Museum, Jinzhou, China
MCSNB, Museo Civico di Scienze Naturali di Bergamo "E. Caffi", Bergamo (Italy);
MCZ, Museum of Comparative Zoology, Harvard University, Boston, U.S.A.
MFSN, Museo Friulano di Storia Naturale, Udine (Italy)
MGCL, Musée Géologique Cantonal de Lausanne, Laussanne, Switzerland
MGUH, Geologisk Museum - Statens Naturhistoriske Museum, Københavns
MIC, Contacto: Museo Interactivo de Ciencias, Universidad Nacio-nal de San Luis, San Luis, Argentina
MJML, Museum of Jurassic Marine Life, Kimmeridge, Dorset, UK
MMP, Museo Municipal de Ciencias Naturales 'Galileo Scaglia,' Mar del Plata, Argentina
MPEF-PV, Museo Paleontológico Egidio Feruglio
MPUM, Museo Paleontologico del Dipartimento di Scienze della Terra, Università di Milano, Italy
MTM, Hungarian Natural History Museum, Budapest, Hungary
NAMAL, National Museum of Ancient Life, US
NHMD, Natural History Museum of Denmark, Copenhagen
NHMUK, the Natural History Museum, London, UK
NJU, Nanjing University, Nanjing, China
NMINH/G, National Museum of Ireland, Natural History, Dublin, Ireland
NMT, National Museum of Tanzania, Dar es Salaam, Tanzania
NSM, National Science Museum, Tokyo, Japan
OUMNH, Oxford University Museum of Natural History
PIN, Paleontological Institute, Russian Academy of Sciences, Moscow, Russia
PMOL, Paleontological Museum of Liaoning, Shenyang Normal University, Shenyang, China
PTH, Philosophisch–Theologische Hochschule, Eichstatt, Germany
PURL, National University of La Rioja
PVL, Instituto Miguel Lillo, Tucumán, Argentina
PVSJ, Paleontología de Vertebrados, Museo de Ciencias Naturales, Universidad Nacional de San Juan, San Juan, Argentina
RAM, Raymond M. Alf Museum of Paleontology at The Webb Schools, Claremont, CA, USA
RGM, Nationaal Natuurhistorisch Museum (Naturalis Biodiversity Center), Leiden, The Netherlands
SC, Italian State Collection
SMF, Senckenberg Museum, Frankfurt, Germany
SMNK Staatliches Museum für Naturkunde Karlsruhe, Karlsruhe, Germany
SMNS, Staatliches Museum für Naturkunde Stuttgart, Stuttgart, Germany
SoS, Jura Museum (Solnhofen Sammlung), Eichstätt, Germany
STM, Shangdong Tianyu Museum of Nature, Pingyi, China
TMM, Texas Memorial Museum, Austin, TX, USA
TMP, Royal Tyrrell Museum of Palaeontology, Drumheller, AB, Canada
UA, Université d'Antananarivo, Antananarivo, Madagascar;
ULBRA, Universidade Luterana do Brasil, Canoas, Brazil.
WDC, Wyoming Dinosaur Center, Thermopolis, U.S.A
YHK, Yizhou Museum, China
YPM, Yale Peabody Museum, New Haven, USA.
ZDM, Zigong Dinosaur Museum
ZMNH, Zhejiang Museum of Natural History, Hanzhou, Zhejiang Province, China.

Characters (no ordering or implied weighting):

Dentition

1) **Dentition**: is 0- present; 1- absent
2) **Dentition across dentary and upper jaw is** 0 - isodont; 1 - heterodont
3) **Crown shape in the maxilla**: 0- multicuspid or serrate; 1- monocuspid
4) **Crown shape in the dentary:** 0- multicuspid or serrate; 1- monocuspid
5) **Monocuspid tooth crowns are:** 0 - stout pegs; 1 - robust curved; 2 - short triangulate or lancelote; 3 - short hooks; 4 - long, thin
6) **Bifid apex of the tooth crown** (ch41, Britt, 2018): 0 – absent; 1 – present
7) **Teeth with three to five cusps** (ch33, Della Vacchia, 2009) 0 - present; 1 – absent

8) **Crown topography of multicuspid teeth** (ch44, Britt, 2018) 0 - flat; 1 - bulbous; 2 - blunt
9) **Striations on the tooth enamel** 0 - absent; 1 – present
10) **Premax & max dentition:** 0 - premaxilla and maxilla dentition strikingly different; 1 - premaxilla and maxilla dentition similar in shape and distribution
11) **Number of monocuspid mandibular teeth;** 0 - 8 or less per mandibular rami; 1 - more than 8
12) **Shape of symphysis teeth, crown height relative to base width** (Andres, 2014); 0- less than four times the width; 1- four times the width
13) **Morphologies across both jaws:** 0 - homodont; 1 - two morphologies; 2 – three morphologies; 3 – four morphologies
14) **Contact between teeth in mesial jaw region;** 0 - present; 1 – absent
15) **Dental spacing** (ch60, Vidovic & Martill, 2014); 0 - regular; 1 - packed rostrally; 2- packed mesially; 3 - irregular
16) **Premaxillar diastema spacing** 0 - present 1 – absent
17) **Dentition under antorbital fenestra** 0 - present, 1 - absent
18) **Rostral monocuspid average tooth curvature** 0 - 180º (straight); 1 - below 170º; 2 - below 160º
19) **Enlarged teeth under the dorsal process of the maxilla** (ch67, Vidovic, 2016): 0 - present ; 1 – absent
20) **Position and presence of teeth** (ch43, Wang, 2009), 0 - even distribution; 1 - teeth absent from anterior; 2 - teeth confined to anterior; 3 - toothless
21) **Distance between teeth posterior to the symphysis** (ch62, Vidovic & Martill, 2015) 0 - is approximately equal to tooth width; 1 - is greater than the tooth width; 2 - is less than tooth width
22) **Sharp, short triangular teeth:** 0 - Lanceolate, curving edge with blunt tips; 1 - short, triangulate with straight edges
23) **Dentition under NAOF:** 0 - present; 1 – absent
24) **Monocuspid teeth**: 0 - unchanging between maxilla and premaxilla; 1 - the premaxilla teeth larger than maxilla but retain similar morphology; 2 - premaxilla teeth large labiolingually narrow fangs, maxilla teeth small prisms; 3 - maxillary teeth considerably smaller and stouter to premaxillary fangs; 4 - monocuspid fangs in premaxilla, lower teeth with accentuated susps in maxilla
25) **Edentulous dentary tip:** 0 - present; 1 – absent

Dentary

26) **Mandibular rhamphotheca:** 0 - absent; 1 – present
27) **Mandibular keel** (modified Andres, 2010); 0 - absent; 1 - restricted to rostrum
28) **Articulation point between the skull and mandible** (ch23, Lu, 2006): 0 - under posterior half of orbit or further backwards; 1 - middle of orbit; 2 - anterior half of orbit
29) **Articular facet** (ch103, Vidovic, 2016): 0 - hatchet shaped in line with mandible; 1 - ventrally deflected; 2 - short, stout in line with mandible
30) **Retroarticular process** (ch99, Vidovic, 2014) Constricted posterior expansion of retroarticular process: present - 0; absent – 1
31) **Dentary changes in depth** 0 - depth consistent; 1 - increases distally; 2 - increases proximally; 3 – irregular
32) **The retroarticular process is:** 0 - outstanding, ventrally sloping from the dentary; 1 - on level with the dentary
33) **Rostral end** (Unwin, 2004) 0 - straight or bent dorsally; 1 - bent ventrally
34) **Mandibular/dental fovea or manidbular ridge**: 0 - present; 1 - absent or poorly defined
35) **Dentary curvature**: 0 - straight; 1 - bows dorsally; 2 - bows ventrally; 3 – irregular

36) **Symphysis:** 0 - unfused; 1 - fused to broad "shovel"-like morphology; 2 - making over 30% of rami fused to a sharp point; 3 - semicircular; 4 - sharp, long triangular less than 30% of rami
37) **Caudal dentary elevated in thickness anterior to the retroarticular process;** 0 - absent, 1 - present

Crania

38) **Skull shape** 0 - length four times the skull height or less; 1 - length more than 4 times the height; 2 - more than 5 times the height
39) **Dorsoventrally elongated foramen in the lateral side of dorsal process** (ch10, Britt, 2018) 0 - absent; 1 - present
40) **Maxilla, dorsal (ascending) process, opening caudally to aof/naof:** 0 - 50-60 degrees; 1 - 40-30 degrees; 2 - below 30 degrees
41) **Maxilla-nasal contact**: 0 - broad; 1 – narrow
42) **Premaxilla, maxilla process beneath the naris**: 0 - present, over half of nares length; 1 - less than half of nares length; 2 - absent due to lack of premaxillary ventral contact with the nares
43) **Jugal-lacrimal contact** 0 -in the ventral half of the orbit; 1 - approximately in the middle; 2 - in the dorsal half of the orbit
44) **Jugal extends under the (naso)antorbital fenestra** (116ch, Vidovic, 2016) 0 - by more than half the length of the vacuity; 1 - less than half the length of the vacuity
45) **Jugal, rostrally expanded to nearly totally overlap laterally the maxilla**: 0 - absent; 1 – present
46) **Jugal comes into contact with maxilla** in 0 - the midline or the posterior end of naof; 1 - the anterior end of naof
47) **A prominent ridge running posterior to lacrimal process of jugal**; 0 - present; 1 – absent
48) **Jugal maxillary process;** 0 - same size or shorter than lacrimal process; 1 - much longer than lacrimal process
49) **Processus Quadrojugalis:** 0 - prominent, at least a half size of lacrimal jugal process; 1 - outstanding but smaller than third of lacrimal process; 2 - completely reduced
50) **Angle of the processus lacrimalis relative to ventral margin of jugal**: 0 - below 100^{o}; 1 - above 100^{o} to 130^{o}
51) **Maxilla process of the jugal inclination relative to the ventral maxillary border** (in non-monofenestratan): 0 - 60 to 50 degrees; 1 - 49 - 30 degrees; 2 - below 30 degrees
52) **Quadrate orientation** (ch49, Unwin, 2003, modified): 0 - inclined anteriorly; 1 - vertical or subvertical (90-110°); 2 - inclined backward at 110-135°; 3 - inclined backwards >135°
53) **Inferior temporal fenestra** 0 - large oblate; 1 - rectangular; 2 - thin line; 3 – piriform
54) **Inferior infratemporal fenestra dorsoventral size**: 0 - long axis of orbit larger than if; 1 - long axis of if same as orbit or larger; 2 - long axis of if considerably larger than orbit (0.5)
55) **Inferior temporal fenestra**: 0 - posterior/posteroventral relative to orbit; 1 - ventral relative to orbit
56) **Skull openings, external narial opening, relative size**: 0 - smaller than orbit or antorbital fenestra; 1 - larger than orbit or antorbital fenestra
57) **Angle of opening of the frontal median notch facet for the dorsocaudal premaxillary bone:** 0 - Above 30 degrees; 1 - Below 30 degrees
58) **Skull openings, antorbital fenestra, position**: 0 - lies level with the naris; 1 - lies partially or totally lower than the naris
59) **Skull openings, antorbital fenestra, shape**: 0 - length more than twice the height; 1 - length twice the height or less

60) **AOF and nares: 0** - separate; 1 - confluent antorbital fenestra
61) **Skull openings, orbit, relative size** (ch14, Unwin, 2003): 0 - larger than antorbital fenestra; 1 - smaller than antorbital fenestra
62) **Orbit shape** 0 - rounded; 1 - sub-rounded/angular/piriform
63) **Supraorbital process intrudes into the orbit** (107ch, Vidovic, 2016) 0- present ; 1 – absent
64) **Premaxillary sagittal crest position** (ch15, Wang, 2009): 0 - absent; 1 - confined to the anterior portion of the skull; 2 - starting anterior to the anterior margin of the nasorbital
65) **Nasal bar in nasorbital fenestra:** 0 - present; 1 – absent
66) **Recess anterior to antorbital fenestra;** 0 - absent; 1 – present
67) **Jugal body ventral to the orbit:** 0 - thin and concave; 1 - stout, short and robust with undulating ventral margin, large triangular orbit margin; 2 - stout, short with flat ventral margin; 3 - long, thin and convex; 4 - rectangular, tall with round ventral orbit margin
68) **Nares size:** 0 - large triangular, 1 - tear shaped; 2 - thin, elongate line
69) **NAOF** 0 - same height as orbit; 1 - taller than orbit height
70) **External Naris ventral margins dorsal & ventral** (Andres, 2010): 0 - acute; 1 - subparallel

Internal cranial features

71) **Interpterygoid vacuity makes up** 0 - over 20% of total palatal length; 1 - under 20% of total palatal length
72) **Choana placement relative to the orbit** 0 - in preorbital region; 1 - ventral to orbit or postorbital
73) **Ectopterygoid position relative to medial of vomers** - 0 - 90^{o} or within the range; 1 - 70 to 40^{o}; 2 - 40^{o} or less
74) **Basipterygoid**; 0- wide 60-100 degrees; 1- narrow 25 - 40 degrees o; 2 - robust, confluent plate
75) **Endocast profile**; 0 - straight; 1 - caudally dipping ventrally
76) **Cerebrum on level relative to the flocculus:** 0 - on the same level; 1 - flocculus on level with ventral half relative to cerebrum
77) **Optic lobe relative to cerebrum**: 0 - large, around 50% of surface area; 1 - reduced, less than 50% of surface area of cerebellum
78) **Ceratobrachialis fuse anteriorly into Y shape**: 0 - absent; 1 – present
79) **Ceratobranchial/skull length ratio** (based on values by Jiang, 2020); 0 - less than 20%; 1 - over 20 to 50%; 2 - 50% or more

Post-crania – vertebral series

80) **Total proxo-distal skull length versus total vertebral dorsum and sacral lengt**h: 0 - skull 50% or less of sacral-dorsal length; 1 - skull over 50% of sacral-dorsal length; 2 - skull as long as sacrum and dorsum if not longer
81) **Postexapophyses on cervical vertebrae** (Kellner, 2003): 0 - absent; 1 – present
82) Notarium: 0 - absent 1 – present
83) **Midcervical ribs** (ch26, Unwin, 2003; ch46, Kellner, 2003) 0 - long, column supported by filiform processes; 1 - reduced or absent
84) **Dimensions of the cervical vertebra, width over length;** 0 - 0.9 or above; 1 - 0.8-0.6; 2 - 0.6-0.5; 3 - 0.4 or less
85) **Neural spine of the mid-cervical vertebrae** (ch47, Kellner, 2003): 0 - tall, blade-like 1 - tall, spike-like 2 - low, blade-like 3 - extremely reduced or absent
86) **Combined dorsal and sacral vertebral series, length relative to ulna length** (Unwin, 2003): 0 - longer than ulna length; 1 - at most ulna length.

87) **Caudal vertebrae, length of the caudal segment of the vertebral column in respect to the dorsal segment** (ch27, Unwin, 2003): 0 - longer; 1 – shorter
88) **Caudal vertebrae, number** (Kellner, 2003): 0 -more than 15; 1 - at most 15.
89) **Caudal vertebrae, elongation** (ch58, Britt, 2018): 0 - short, longest caudal centrum < 2.5 times longer than a mid-dorsal centrum; 1 - elongate > 2.5 times longer than a mid-dorsal centrum, robust and tabular 2 - elongate > 2.5 times longer than a mid-dorsal centrum, robust and tabular thin elongate rods
90) **Caudal vertebrae, filiform processes of caudal zygapophyses** (ch30, Unwin, 2004) - 0 - absent; 1 - present;
91) **Vane:** 0 - diamond or triangular, restricted to caudal end; 1 - bulbous, numerous oval soft tissue elements running from caudal mid-section

Trunk & Pubic region

92) **Scapula length** (ch49, Kellner, 2003); 0 - subequal or longer than coracoid; 1 - scapula shorter than coracoid sca/cor>0.8); 2 - shorter coracoid (sca/cor<0.80)
93) **Articular region of scapulacoracoid posterior to supraglenoid buttress**; 0 - small; 1 - wide, distorting profile of coracoid
94) **Shape of scapula:** 0 - slender concave rod; 1 - slender concave rod with dorsal profile interrupted by extensive articular region; 2 - straight, stout rod
95) **Coracoid, shape** (Sereno, 1991, char. W, modified by Britt, 2018) 0 - with (dorsoventrally) elongated and broad shaft, flattened at midshaft; 1 - with strut-like shaft, slender and cylindrical at midshaft, expanded distally
96) **Humerus, proximal articular surface**: (ch233, Kammerer, 2020): 0 - continuous with the deltopectoral crest ; 1 - separated by a gap from the deltopectoral crest
97) **Cristopine** (ch53, Kellner, 2003) 0 - absent; 1 shallow, elongated
98) **Lateral process on the caudal end of sternal plate** 0 - absent; 1 – present
99) **Supraglenoidal buttress**; 0 - proximal shaft of scapula; 1 - closer to acrocoracoid process
100) **Ischiopubic plate** (ch107, Andres, 2008): 0 - unexpanded; 1 – present
101) **Caudal end of sternal plate:** 0 - straight; 1 - tapering to a triangulate caudal point
102) **Prepubis proximal end:** 0 - lobate; 1 - trapezoidal with strongly defined undulating or straight edges; 2 - large with blunt "mushroom-shaped" end; 3 – simple, triangulate
103) **Ilium, anterior (=preacetabular, =cranial) process:** (ch269, Kammerer, 2020)' 0, short and does not extend anterior to the acetabulum; 1, long and extends anterior to the acetabulum
104) **Caudal process of the ischium**; 0 - sub-rectangular or sub-trapezoidal in lateral view; 1 - pointed, oblate in lateral view
105) **Vacuity between the postacetabular process & ischiopubic plate:** 0 - large, circular; 1 - triangulate; 2 - narrow incision

Hindlimb elements

106) **Femur, anterior trochanter (=M. iliofemoralis cranialis insertion)** (ch308, Kammerer, 2020):' 0 absent present and forms a steep margin with the shaft but is completely connected to the shaft; 1, present and forms a steep margin with the shaft and separated from the shaft by a marked cleft
107) **Femoral neck shape** (Andres, 2014): 0 - indistinct; 1 – constricted
108) **Fibula, relative length** (ch8, Unwin, 2003): 0 - similar length as tibia 1 - shorter than tibia, not reaching the tarsus
109) **Femur, anterolateral side of the femoral head** (ch 310, Kammerer, 2020): '0, smooth, featureless ; 1, ventral emargination present,
110) **Femur, crista tibiofibularis** (fibular condyle of Sereno & Arcucci 1994)(ch326, Kammerer, 2020): 0 smaller or equal in size to the medial condyle; 1, larger than the medial condyle

111) **Femur distal end, epicondyles size** (Andres, 2014): (0) reduced and confluent with distal condyles; (1) expanded into distinct distal flanges;
112) **Greater trochanter of the femur** (ch218, Andres, 2014): 0 - reduced; 1 - distinct process; 2 - curved hook or sizeable triangular;
113) **Femur distal epiphysis**: 0 - distally enlarged; 1 - same width as diaphysis; 2 - fanning, hatchet shaped expansion
114) **Femur diaphysis** - 0 - sigmoidal; 1 - convex or concave 2 – straight
115) **Metatarsals, relative length of metatarsal IV**: 1 - longer than metatarsal I; 2 - sub-equal in length to metatarsal I; 3 - shorter than metatarsal I
116) **Tibia to Humerus**; 0 - tibia same or bigger than humerus; 1 - humerus bigger than tibia
117) **Pedal digit V, phalangeal count** (ch73, Kellner, 2003): 1 - three or four phalanges; 2 - two phalanges; 3 - one or none (extremely reduced)
118) **Pedal digit V, phalanx 2, shape**: 0 - straight or slightly arched; 1 - curved proximally; 2 - bent (angled) at mid-length
119) **Femur, length relative to metacarpal IV length** (after Kellner, 2003): 0 - at least twice metacarpal IV length (fe/mcIV > 2.00); 1 - less than metacarpal IV length (fe/mcIV < 2.00)
120) **Metatarsal III, length relative to tibia length** (after Kellner, 2003): 0 - more than one-third tibia length (mtIII/ti > 0.33); 1 - at most one-third tibia length (mtIII/ti ? 0.33)
121) **Metatarsal IV length** (ch395, Kammerer, 2020): 0 - longer than metatarsal II; 1 - subequal shorter than metatarsal II
122) **Metatarsal IV** (ch 393, Kammerer, 2020); 0 - longer than metatarsal III; 1 - same lenght or shorter than metatarsal III
123) **Metatarsal V** - 0 - >50% size of MTIV, stout hatchet-shaped and robust, almost twice the thickness of MtIV, followed by elongate digits; 1 - lobate, thinner MTV, with thickness similar to that of MTIV, followed by elongate digits; 2 - lobate to tear-shaped, <twice the thickness of MtIV, followed by reduced digits
124) **Metatarsal V, dorsal prominence separated from the proximal surface by a concave gap** (ch, 397. Kammerer, 2020): 0 - absent [outgroup], 1 – present

Forelimb

125) **Ulna, proportions with tibia** (ch61, Lü et al., 2012): 0 - less than 0.9; 1 - 0.9-1.2; 2 - 1.2-1.4; 3 - >1.4
126) **Ulna distal tuberculum position** (Ch197, Andres, 2014): 0 - middle of the distal end; 1 - ventral part of the distal end;
127) DPC is; 0 - larger than ulnar crest; 1 - same size as ulnar crest; 2 - smaller than ulnar crest
128) **Ulnar crest curves in convex fashion proximally:** 0 - absent, 1 – present
129) **Ulna, length relative to humerus**: 0 - less than 1.5 times length of humerus; 1 - 1.5 times length of humerus or more
130) **Humeral diaphysis angle**; 0 - 180, straight; 1 - 170-160º curvature; 2 - below 160º
131) **Humerus, proximal articular surface**: (ch233, Kammerer, 2020): 0 - continuous with the deltopectoral crest ; 1 - separated by a gap from the deltopectoral crest
132) **Humerus pneumatic foramen on a proximal end ventral surface** (ch185, Andres, 2014): 0 - absent; 1 – present
133) **Humerus distal end anterior aspect pneumatic foramen** (ch189, Andres, 2014): 0 - absent; 1- present
134) **DPC neck constriction** 0 - absent; 1 – present
135) **DPC ventral margin**- 0 - shallow extension from diaphysis with flat proximal margin; 1 - proximally extending, steeply inclining lobe; 2 - laterally extending hatchet

136) **DPC dorsal surface**: 0 - straight or concave; 1- convex
137) **DPC proximal surface**: 0 - straight; 1 - undulating, with proximal notch seperating ulnar and deltopectoral crests
138) **Muscle scar or a process on dorsal humeral surface:** 0 - absent; 1 - present
139) **Manual ungual, size relative to pedal ungual**: 0 - less than twice the size of pedal ungual; 1 - at least twice the size of pedal ungual;
140) **Metacarpals I-III distalends, positions** (ch138, Andres, 2012) : 0 - disparate; 1 - approximate;
141) **Metacarpus, relative length of elements I-III**: 0 - metacarpal I < metacarpal II < metacarpal III; 1 - metacarpal I < metacarpal II = metacarpal III; 2 - all the same length
142) **Metacarpus, metacarpal IV-humerus ratio** (ch29; Unwin, 2003): 0 - less than 35%; 1 - more than 35% but less than 80%; 2 - more than 80%
143) **Proximal metacarpal**: 0 - extended, broad, 1 - similar in width to the diaphysis
144) **Metatarsal V, phalanges** (ch399, Kammerer, 2020): 0 - without phalanges, metatarsal tapers to a point [outgroup condition]; 1 - fully developed phalanx
145) **Pteroid bone, elongation**: 0 - 1/6 ulnar length or less; 1 - 1/6-2/5 ulnar length; 2 - more than 2/5 ulnar length
146) **Pteroid, shape**: 0 - angled at midsection; 1 - stout hook; 2 - straight and tapered with expanded proximal end; 3 - straight with expanded ends; 4 - curved slender rod; 5 - curved and not tapered;
147) **Pteroid:** 0 - absent; 1 – present
148) **Wing phalanx 1, relative size** (ch45, Unwin, 2004): 0 - less than 35% wing finger length; 1 - 35% wing finger length or more
149) **Wing phalanx 1, length relative to wing metacarpa**l (ch66, Kellner, 2003): 0 - phalanx over twice the length of the metacarpal; 1 - phalanx less than twice the length of the metacarpal
150) **Wing phalanx 2, length relative to ulna** (Unwin, 2003): 0 - shorter than ulna; 1 - as long as ulna or longer
151) **Wing phalanx 2, length relative to wing phalanx 1** (ch68, Kellner, 2003): 0 - phalanx 2 about the same size or longer than phalanx 1; 1 - phalanx 2 shorter than phalanx 1
152) **Wing phalanx 3, length relative to wing phalanx 1** (ch69, Kellner, 2003; ch105, Andres, 2008): 0 - phalanx 3 about the same length or longer than phalanx 1; 1 - phalanx 3 shorter than phalanx 1
153) **Wing phalanx 3, length relative to wing phalanx 2** (ch70, Kellner, 2003, modified): 0 - phalanx 3 about the same length or longer than phalanx 2; 1 - phalanx 3 shorter than phalanx 2
154) **Wing phalanx 4, size:** 0 - more than 30% the length of the wing phalanx 3; 1 - extremely reduced (less than 30% the length of wing phalanx 3) or lost
155) **WP4** 0 - reduced; 1 - straight; 2 - concave or convex